

# CHEMISTRY

## A European Journal

A Journal of



### Accepted Article

**Title:** Fluorescence Lifetime Imaging and Super resolution microscopies shed light on the directed- and self-assembly of functional porphyrins onto carbon nanotubes and flat surfaces

**Authors:** Boyang Mao, David González Calatayud, Vincenzo Mirabello, Haobo Ge, Benjamin J Hodges, Robert M. J. Jacobs, Ashley M. Shepherd, José Alberto Ribeiro Martins, Navaratnarajah Kuganathan, Jorge Bernardino De La Serna, Stanley W. Botchway, and Sofia Ioana Pascu

This manuscript has been accepted after peer review and appears as an Accepted Article online prior to editing, proofing, and formal publication of the final Version of Record (VoR). This work is currently citable by using the Digital Object Identifier (DOI) given below. The VoR will be published online in Early View as soon as possible and may be different to this Accepted Article as a result of editing. Readers should obtain the VoR from the journal website shown below when it is published to ensure accuracy of information. The authors are responsible for the content of this Accepted Article.

**To be cited as:** *Chem. Eur. J.* 10.1002/chem.201605232

**Link to VoR:** <http://dx.doi.org/10.1002/chem.201605232>

Supported by  
**ACES**

WILEY-VCH

# Fluorescence Lifetime Imaging and Super resolution microscopies shed light on the directed- and self-assembly of functional porphyrins onto carbon nanotubes and flat surfaces

Boyang Mao,<sup>#[a],[b]</sup> David G. Calatayud,<sup>#[a]</sup> Vincenzo Mirabello,<sup>#[a]</sup> Navaratnarajah Kuganathan,<sup>[c]</sup> Haobo Ge,<sup>[a]</sup> Robert M. J. Jacobs,<sup>[d]</sup> Ashley M. Shepherd,<sup>[d]</sup> José Alberto Ribeiro Martins,<sup>[e]</sup> Jorge Bernardino De La Serna,<sup>[f]</sup> Benjamin J. Hodges,<sup>[a]</sup> Stanley W. Botchway,<sup>[f]</sup> and Sofia I. Pascu<sup>\*[a]</sup>

**Abstract:** Functional porphyrins have attracted intense attention due to their remarkably high extinction coefficients in the visible region and potential for optical and energy-related applications, ranging from biosensors or photovoltaic based devices. Two new routes to functionalized SWNTs have been established using a bulky Zn(II)-porphyrin featuring thiolate groups at the periphery. We probed the optical properties of this Zinc(II)-substituted, bulky aryl porphyrin and those of the corresponding new nano-composites with single walled carbon nanotube (SWNTs) and coronene, as a model for graphene. We report hereby on: (i) the supramolecular interactions between the pristine SWNTs and Zn(II)-porphyrin by virtue of  $\pi$ - $\pi$  stacking, and (ii) a novel covalent binding strategy based on the Bingel reaction. We investigated the nature of the porphyrin aggregates forming on flat surfaces by Steady-state and time-resolved fluorescence emission spectroscopies and imaging techniques including fluorescence lifetime imaging microscopy (FLIM) together with Atomic Force Microscopy (AFM) and Super Resolution Stimulated Emission Depletion microscopy (STED). The functional porphyrins used acted as dispersing agent for SWNTs and the resulting nanohybrids showed improved dispersibility in common organic solvents with respect to the pristine nanotubes. Characterization techniques were carried out in the thin film phase on a variety of surfaces, leading to the prediction that supramolecular polymerization and host-guest functionalities control the fluorescence emission intensity as well as the fluorescence lifetime properties. For the first time, X-ray photoelectron spectroscopy

(XPS) studies highlighted the differences in the covalent versus non-covalent attachments of functional metalloporphyrins to SWNTs. Gas phase density functional theory (DFT) calculations (implemented in the Cambridge Serial Total Energy Package CASTEP) indicated that the Zinc(II) porphyrin interacts non-covalently with SWNTs to form a donor-acceptor complex. Taken together, the techniques applied here for the characterization work link findings in the solution, surface and gas phase. The appendage of the porphyrin chromophore to the surface of SWNTs (covalently, *via* a directed assembly method based on dynamic covalent chemistry) affects the absorption and emission properties of the hybrid system to a greater extent than in the case of the supramolecular functionalization of the SWNTs surface (non-covalently, *via* donor-acceptor self-assembly). This represents a synthetic challenge as well as an opportunity in the design of functional nanohybrids for future sensing and optoelectronic applications.

## Introduction

Since the discovery of single-walled carbon nanotubes (SWNTs)<sup>[1]</sup> there has been a sustained interest in this material from both academic and industrial research perspectives. This is due to the fact that its rigid rod-like tubular structure, coupled with a highly delocalized extended  $\pi$ -electron system, confers its unique mechanical and electronic properties thus offering promises of technological advances.<sup>[2]</sup> Ongoing studies show that, upon functionalization of SWNTs with small molecules, it is possible to develop prototype optoelectronic and photovoltaic devices.<sup>[3]</sup> Thus, the interactions between fluorescent molecules, as well as semiconductive polymers, and the aromatic surface of SWNTs have attracted significant interest due to the potential application of these new nanohybrids, particularly in solar cells.<sup>[4]</sup>

One of most attractive properties of SWNTs is the possibility to chemically modify their surfaces by two general approaches: covalent or non-covalent synthetic methodologies. The intrinsic  $sp^2$  nature of the C-C bond of the SWNT allows reaction with organic molecules bearing specific functional groups that react with the outer walls of the tubular material. Porphyrins have been used as versatile chromophores having the ability to act as dispersing agents for carbon nanomaterials and to decorate C<sub>60</sub>,<sup>[5]</sup> carbon nanotubes<sup>[6]</sup>, graphene oxide<sup>[7]</sup> or nanohornes<sup>[8]</sup> in artificial photosynthetic devices.<sup>[9]</sup> SWNTs can interact *via* aromatic stacking with electron-rich planar molecules resulting in supramolecular donor-acceptor complexes. Such molecules including porphyrins, planar, electron-rich, aromatic species are characterized by remarkably high extinction coefficients in the visible region. Tailor-made porphyrins designed to include thiol units suitable for dynamic covalent chemistries have been

# These authors contributed equally to this work.

[a] Dr. B. Mao, Dr. D. G. Calatayud, Dr. V. Mirabello, Dr. H. Ge, B. J. Hodges, Prof. S. I. Pascu  
Department of Chemistry  
University of Bath  
Claverton Down, BA2 7AY, Bath, UK  
E-mail: s.pascu@bath.ac.uk

[b] Dr. B. Mao  
National Graphene Institute and School of Physics and Astronomy  
The University of Manchester  
Booth Street East, Manchester M13 9PL

[c] Dr. N. Kuganathan  
Department of Materials  
Imperial College London  
South Kensington, London SW7 2AZ, UK

[d] Dr R. M. J. Jacobs, Dr. A. M. Shepherd  
Department of Chemistry  
Chemistry Research Laboratory, University of Oxford  
Mansfield Road, Oxford OX1 3TA, UK

[e] Dr. J. A. Ribeiro Martins  
Centro de Engenharia Biológica and Departamento de Química  
Universidade do Minho  
Campus de Gualtar, 4710-057 Braga, Portugal

[f] Prof. S. W. Botchway, Dr. J. Bernardino De La Serna,  
Central Laser Facility, Rutherford Appleton Laboratory  
Research Complex at Harwell  
STFC Didcot OX11 0QX, UK  
Supporting information for this article is given via a link at the end of the document.

designed and their ability to recognize fullerenes or small molecular acceptors such as naphthylidimides in a controlled way has been demonstrated.<sup>[10]</sup> Such nanohybrids have the potential to offer valuable new technologies in the field of nano-optoelectronic devices for energy conversion, sensing and biological applications.<sup>[4c, 11]</sup> The recent work by Strano and collaborators has demonstrated the potential of non-covalent sensors based on SWNTs in biology.<sup>[13]</sup> Thiol-derivatized functional Zn(II) porphyrin-based systems<sup>[7]</sup> have not been investigated thus far in the context of generating new SWNTs adducts with targeted optical properties. The combination of the unique electron transport properties of the SWNTs together with the promising photo-chemical properties of tailor-made functional porphyrins could render their new adducts as potential candidates for dispersible solid state scaffolds in nano-optoelectronic devices and bio-sensing. Crucially, using X-ray

photoelectron spectroscopy (XPS), as well as fluorescence imaging techniques we also demonstrated here that the formation of the porphyrin-SWNTs supramolecular networks can be controlled through directed and self-assembly giving rise to extended nano-structures with interesting optical properties.

We characterized these materials in a thin film environment using fluorescence lifetime measurements *via* time correlated single-photon counting (TCSPC) combined with multi-photon laser scanning confocal microscopy: this allows us to gain detailed information on the environment of the fluorophore upon immobilization within the nanomaterial hybrid and estimate the influence of the different linking strategies on the emerging materials' optical properties by observing their quenching characteristics in solution and in the solid state.<sup>[7, 12]</sup>

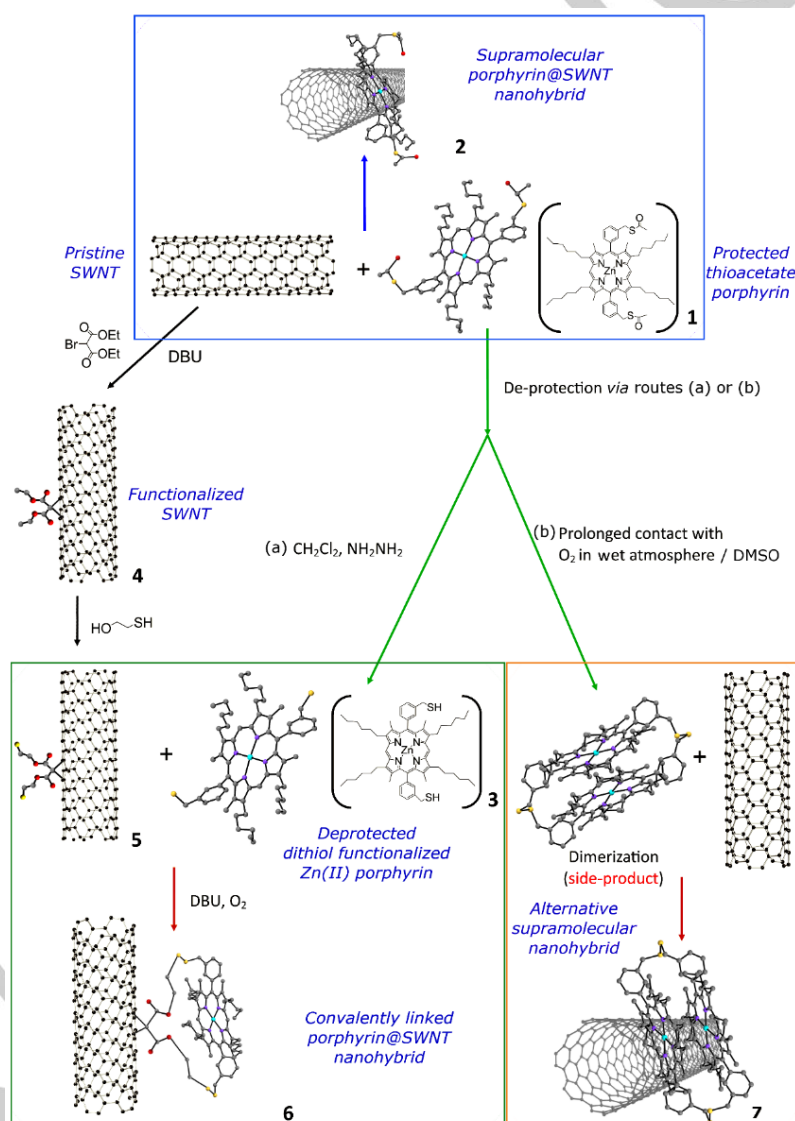


**Figure 1.** Schematic diagram of the formation of covalently and non-covalently linked Zn(II)-porphyrin@SWNTs hybrids (2) and (6). (Element Colour: oxygen – red, sulphur – yellow – nitrogen – purple, light blue – zinc and grey – carbon. The structure of the disulphide linked side-product was obtained via single crystal X-ray diffraction, a ball and stick representation is used for clarity)

Characterization approaches rely on several different efficient and novel physical measurement methods coupled with multi-scale microscopies to identify unequivocally the existence of a covalent and non-covalently linkage between small organic molecules and carbon nanomaterials. The approach reported hereby can become a general methodology for achieving control of photochemistry and sensing capabilities of a wide range of optical and energy materials by tailoring the nature of the interactions between components using directed- and self-assembly processes in solution and thin film.

## Results and Discussion

### *Synthesis and structural investigations: Single crystal X-Ray Diffraction and Super resolution imaging*

We report on the synthesis of novel SWNT-porphyrin nanohybrids. The porphyrin of choice is a member of a family of substituted aryl porphyrins known to be soluble in most common solvents, e.g. toluene, dichloromethane and ethanol, and easily derivatized (Compound **1**). New functional materials were synthesized *via* directed- and self- assembly methods: the synthetic strategies involve, respectively, a new dynamic covalent route (based on the thiols-disulphide exchange involving a Zn(II) porphyrin dithiolated synthon and a thiolated SWNTs surface) and a simple and straight forward non-covalent linking strategy.

The non-covalent, outer surface modification of SWNTs was carried out *via* supramolecular  $\pi$ - $\pi$  interaction of the aryl thioacetate-functionalized hexyl substituted Zn(II)-porphyrin (**1**) (Figure 1) in a one-step process, leading to the formation of complex **2**.

For the generation of the covalently linked system, the surface of the SWNTs was first modified to incorporate a thiol group capable of reacting with the -SH groups of **3** and generating S-S disulphide bridges. The Bingel reaction was used to generate thiol groups on the surface of the nanotubes, which in turn can be zate the covalent appendage<sup>[14]</sup> to the SWNTs surface (Figure 1) *via* thiol-disulfide exchanges.

The Zn(II)-porphyrin (**1**) has been specifically chosen to incorporate four hexyl chains on the exocyclic positions of the macrocycle ring to enhance its solubility in common organic solvents. Moreover, two aryl thioacetate side groups have been included with the intention to help direct the dynamic covalent linkage of porphyrin to the thiol-functionalized outer surface of the SWNTs. For the synthesis of the free porphyrin and zinc(II) porphyrin on a milligram scale, suitable for further synthetic manipulations, the general reaction methodology proposed by Twyman and Sanders was adapted.<sup>[15]</sup> This method involved 1-

iodohexane, pentane-2,4-dione and benzyl 3-oxobutanonate as starting materials, and is described elsewhere.<sup>[16]</sup> The hexyl-derived pyrrole acts as the basic building unit from which the functional porphyrins are assembled.<sup>[17]</sup> This synthetic method allowed the incorporation of a versatile range of peripheral groups at the porphyrin core, including extended alkyl chains or bulky substituents. The nature of the metal center can be further modified to tune their ability in host-guest recognition of relevance for photovoltaic applications.

The resulting porphyrins were fully characterized in solution and in the solid state, and X-ray diffraction studies showed that indeed, under conditions specific for dynamic covalent chemistry, the thiol groups lead to the formation of disulfie-bridged dimer. This new compound could be isolated and fully characterized (ESI). Diffusion Ordered Spectroscopy (DOSY) was employed to explore the possibility that porphyrins of type (**1**) self-aggregate in the solutions used to perform experiments on the NMR scale. This method was deemed a convenient spectroscopic tool as it has been already applied in supramolecular chemistry to identify inter- and intra-molecular self-assembled aggregates and aid the understanding of host-guest interactions in solution.<sup>[18]</sup> Here, we estimated the experimental diffusion coefficients ( $D_{exp}$ ) to predict the tendency of porphyrin molecules of type (**1**), and of its free-base precursor to self-aggregate.<sup>[19]</sup> DOSY spectra of Zn(II)-porphyrin (**1**) and of its free-based porphyrin precursor were acquired at 298 K and are shown in Figure 2 and ESI (Figure S7). The  $D_{exp}$  for Zn(II)-porphyrin (**1**) and metal-free porphyrin precursor were estimated to be  $1.62 \times 10^{-9} \text{ m}^2 \text{ s}^{-1}$  and  $4.57 \times 10^{-10} \text{ m}^2 \text{ s}^{-1}$  respectively. These findings indicate the low tendency of these porphyrins to self-aggregate in solution at the concentration needed to obtain an NMR spectrum (5 mM). This is consisted with previous reports for simpler porphyrin systems such as Tetraphenylporphyrin (TPP).<sup>[19]</sup> It has already been shown that Zn-porphyrins can be functionalized and their self-assembly can generate nano-rings of 5-60 porphyrin units.<sup>[17a, 20]</sup> Earlier observations by AFM or STM measurements performed on drop-casted solutions show that such supramolecular architectures can be described as nano-crystalline aggregates of porphyrins having a shape of a ring or tower, with sizes varying in the range of hundreds of nanometers, depending on the imaging method used to evaluate the size.<sup>[7, 11c, 21]</sup>

Confocal fluorescence imaging of such films formed on borosilicate glass (when a solution of the chromophore was allowed to dry slowly onto a glass surface, *vide infra* and ESI) also seemed to suggest that a self-assembled process is likely to occur, but the precise shape or size could not be asserted due to the low resolution. We were intrigued by the objects formed on insulating surfaces (e.g. mica or borosilicate glass) for the Zn(II) porphyrins and by their optical emissive properties.

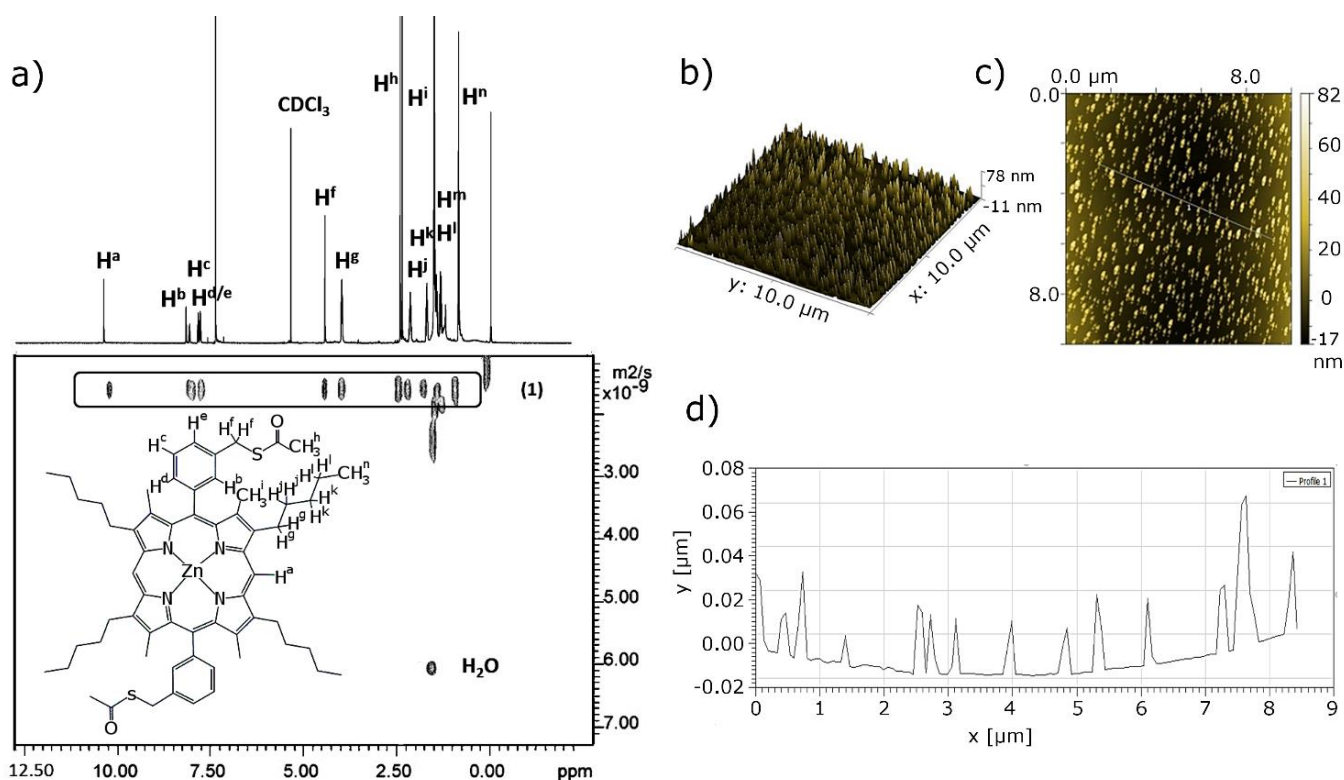


**Figure 2.** a)  $^1\text{H}$  DOSY NMR spectrum (500 MHz, 298 K,  $\text{CDCl}_3$ ) of Compound **1**. Diffusion coefficient =  $1.62 \times 10^{-9} \text{ m}^2 \text{ s}^{-1}$  which limited ability of this Zn(II) porphyrin to aggregate in solution even at ca 5 mM (needed to record a spectrum); b) 3D TMAFM image of Zn(II)-porphyrin (compound **1**) self-assembly on mica. For the TM AFM measurement, Zn(II)-porphyrin sample was prepared by using the spin coating at 3000 rpm of the Zn(II)-porphyrin solution ( $18.3 \mu\text{M}$  in  $\text{CHCl}_3$ ) onto a  $2 \text{ cm}^2$  mica substrate. c) Tapping mode AFM image of Zn(II)-porphyrin self-assembly crystal; d) Profile analysis showing the heights of line.

Super resolution imaging, additionally to single- and multi-photon confocal fluorescence imaging techniques, was employed to further characterize the sub-structure morphologies of the tower-like aggregates observed for (**1**) on surfaces, and thus aid our understanding thereof. These optical imaging experiments in thin film were crucially necessary since solution experiments by DOSY suggested that at ca. 5 mM concentration needed to record NMR spectroscopy in  $\text{CDCl}_3$ , little convincing evidence for aggregation was found. Stimulated emission depletion (STED) microscopy with 775 nm depletion laser was used to assess the morphology and the emission properties of the solid aggregates of the Zn(II)-porphyrin (**1**) previously observed by confocal fluorescence as well as AFM (**Figure 3**). Interestingly, STED deconvolution and surface 3D rendered image reveals that such Zn(II)-porphyrin (**1**) microcrystalline cylinders are roughly  $2 \mu\text{m}$  in height. The larger rings of the tubular structures have a thickness of  $611.3 \pm 3.7 \text{ nm}$ , whilst the smaller is  $323.5 \pm 2.7 \text{ nm}$ . The tubular sub-structure is formed of smaller concatenated rings, which grow in size from the bottom to the top. The smallest ones observed were of 50nm diameter and the largest 130nm found both at the top and towards the periphery of the basal plane, and this method does not allow the exploration of aggregates smaller than ca 30 nm. Interestingly, the free base porphyrin precursor only displayed a very weak STED effect, and the size of the porphyrin stacks could not be fully interpreted by this method, whereas the SWNTs

functionalized porphyrins (synthesized as described below) did not yield such an effect at all, and therefore could not be imaged by super resolution under these conditions. The presence of Zn(II) center, together with the thiol-protected aryl groups and the ability to form aromatically stacked aggregates, play a crucial role in mediating the nature of the self-assembly of these porphyrins on insulating surfaces. The application of super resolution, STED, has allowed the observation of these structures on the nanoscopy scale ( $<100 \text{ nm}$ ). As yet, the effect of such 'tower'-like structure formation on the optical properties of the nanomaterial emerging remained unexplored.

As stated above, the pristine strands of SWNTs were subsequently used as template in an attempt to control the formation of such cylindrical supramolecular assemblies of porphyrins offering an alternative synthetic route to the covalent functionalization of SWNTs which has already attracted broad attention in the scientific community.<sup>[9a, 22]</sup>

**Figure 1** shows the reaction scheme of the Zn(II)-porphyrin@SWNTs non-covalent complex (**2**). A dispersion of SWNTs in chloroform and a Zn(II)-porphyrin solution in the same solvent were mixed and stirred for 24 hours at room temperature and the solid nano-composites obtained were collected by nano-filtration and washing with ethanol.

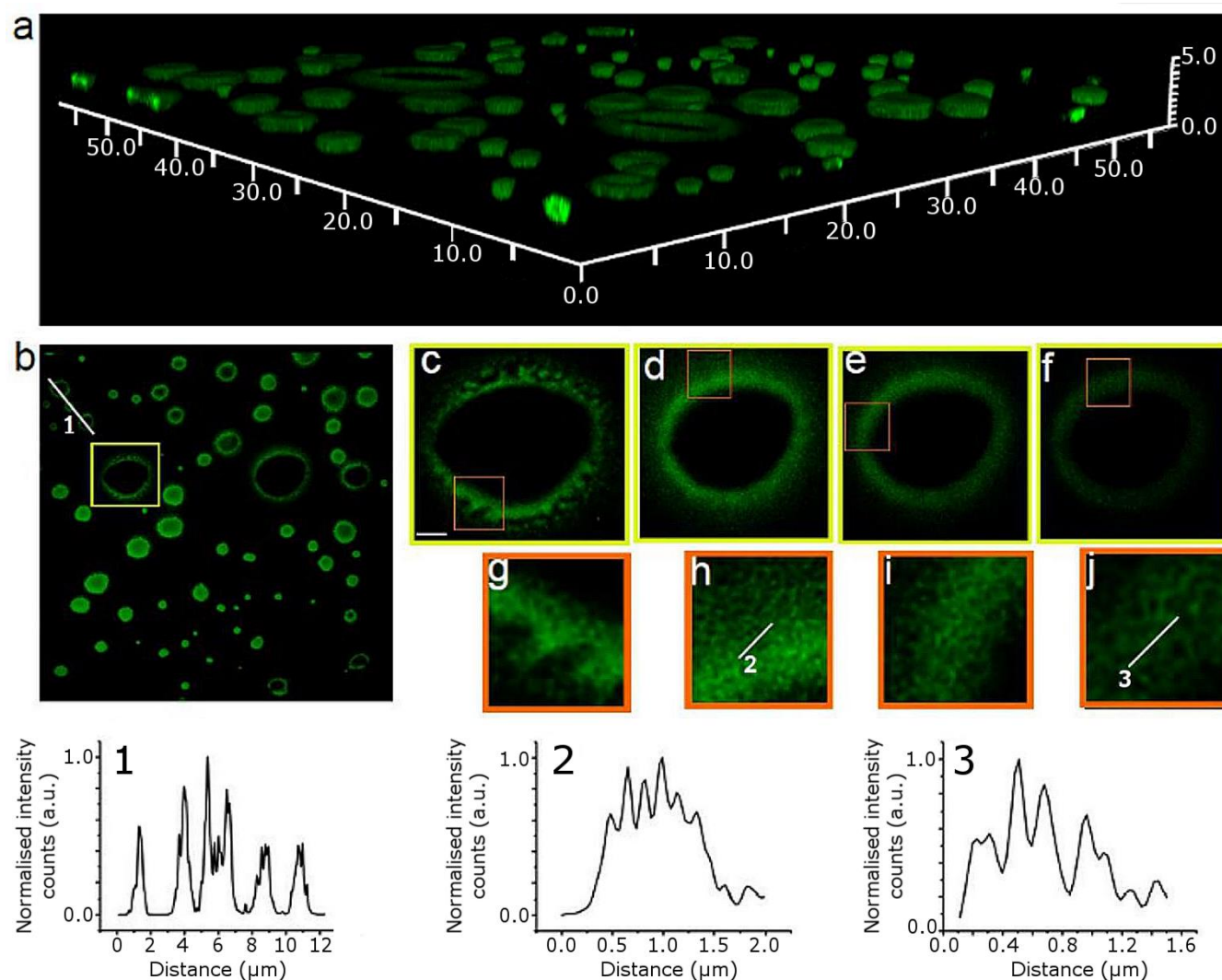


**Figure 3.** Stimulated emission depletion (STED) microscopy of Zn(II)-porphyrin (1) thin film of a  $\text{CHCl}_3$  solution drying out on a borosilicate glass surface,  $\lambda_{\text{ex}} = 488 \text{ nm}$ , STED = 775 nm, laser power intensity = 179 mW,  $\lambda_{\text{em}} = 580 \text{ nm}$ . Scalebar: 10  $\mu\text{m}$ . Top image (a), Deconvolved image of a 3D reconstruction obtained from stacked individual STED images. The image is shown in perspective for better appreciation of the different height of the tubular structures. The X, Y, and Z scales are in  $\mu\text{m}$ . Below, from right to left, deconvolved image of the 3D reconstruction as projected in the XY plane (b). The line profile crossing 3 different tubes is shown in the graph below (1). The highlighted squared region in image (b) is magnified to the right; each image from left to right (c-f), is showing the same tubular structure at different z-planes, with a difference between planes of 300nm, being (c) the lowermost region in contact with the surface, and (f) the uppermost. Below each image can be observed the squared region zoomed in (g-j). The lines profiles drawn in (h) and (j) are represented in the graphs 2, and 3 respectively.

The self-assembly approach provided a simple one-step reaction method leading to the supramolecular adduct (2): the formation of the Zn(II)-porphyrin@SWNTs adduct 2 was likely due to the aromatic stacking between the pyrrole rings of the Zn(II)-porphyrin and the SWNT framework. During synthesis it emerged that the formation of disulfide bridged porphyrin oligomers is favorable over time in the presence of oxygen and in aqueous environments. A disulfide dimer side product featuring two S-S bridges and aromatically stacked porphyrins was isolated and fully characterized (Figure 4 and ESI). Therefore, in the non-covalent linked synthesis strategy, the thioacetate-protected Zn(II)-porphyrin was prepared and used in fresh solutions.

The directed assembly, leading to the disulfide bridged covalent linkages, was achieved as described in Figure 1. Spectroscopic investigations were carried out aiming to probe whether or not this route can lead to a change of the carbon hybridization in the outer wall of the carbon-based material. The subsequent loss of the electronic conjugation, which affects the electron-acceptor or the electron-transport properties was an expected feature of this approach.<sup>[22]</sup> In order to achieve a covalently linkage between SWNTs and the complex (3), a four-step path reliant on dynamic exchange known to occur between thiol-disulfide was devised (Figure 1).

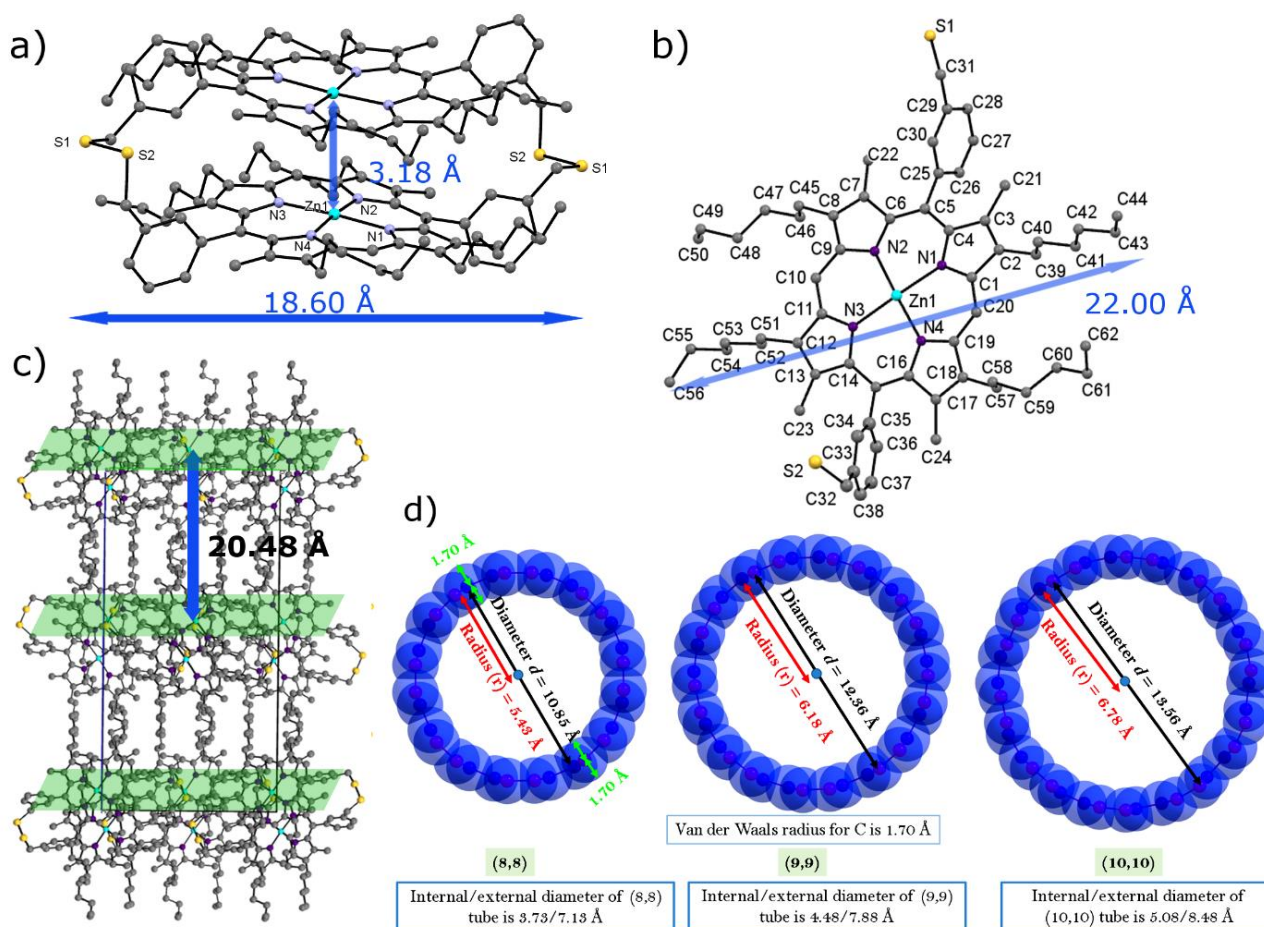


**Figure 4.** Molecular structure determinations by synchrotron single-crystal X-ray diffraction: a) the emerging side-product Zn(II)-porphyrin as a disulfide-bridge dimer, b) cell packing diagram, of the Zn(II)-porphyrin disulfide dimer, view over axis a. Hydrogen atoms were removed for clarity and c) DFT optimised structures of model (8,8), (9,9) and (10,10) SWNTs.

Chemical modifications of both compound (**3**) and SWNTs were introduced prior to the start of the thiol-disulphide reaction. These aimed to allow the control of the porphyrins position on the surface of the SWNTs. First, as shown in Figure 1, (Step *i*) SWNT cyclopropanation reaction was achieved in the presence of diethyl bromomalonate and 1,8-diazabicyclo[5.4.0]undecene (DBU). The resulting mixture led to the (outer surface) modified SWNTs (**4**). Next, (Step *ii*) SWNTs strands were further derivatized by reacting (**4**) with 2-mercaptoethanol, which acts as both liner spacer and thiol-precursor linker. At Step *iii*, Zn(II)-porphyrin (**1**) was deprotected, by treatment with excess hydrazine to obtain the thioacetyl de-protected Zn(II)-porphyrin (**3**). Finally, (Step *iv*) compounds (**3**) and (**5**) were assembled, aiming to covalently coupled their thiols appendages in the presence of DBU thus yielding the novel nanohybrid disulphide bridged adduct (**6**).

#### Microscopy investigations of the SWNT hybrids by AFM and TEM

The morphological properties of the two products, denoted Complexes (**2**) and (**6**), were evaluated and compared by Tapping mode AFM (TM AFM) and TEM. In order to investigate the different electron-acceptor or electron-transport properties in covalent and non-covalently linked Zn(II)-porphyrin@SWNTs complexes, UV-vis, steady-state time-resolved fluorescence emission studies, together with Raman spectroscopy, were performed. TM AFM measurements were carried out to further study the SWNTs nanohybrids and compare their aggregation with that observed in Zn(II) porphyrins. Interestingly, for SWNTs, HOPG worked best as the substrate of choice for AFM images (ESI). The AFM images in Figure 5 (a) and (b) show that the covalent Zn(II)-porphyrin@SWNTs nanohybrids is relatively well dispersed in solution and its diameter is ca 11 nm. The AFM images in Figure 5 (d) and (e) indicate that non-covalent Zn(II)-porphyrin@SWNTs nanohybrids are ca. 9 nm in diameter. The slight difference in diameter between the non-covalently linked and covalently linked nanohybrids is likely a direct consequence

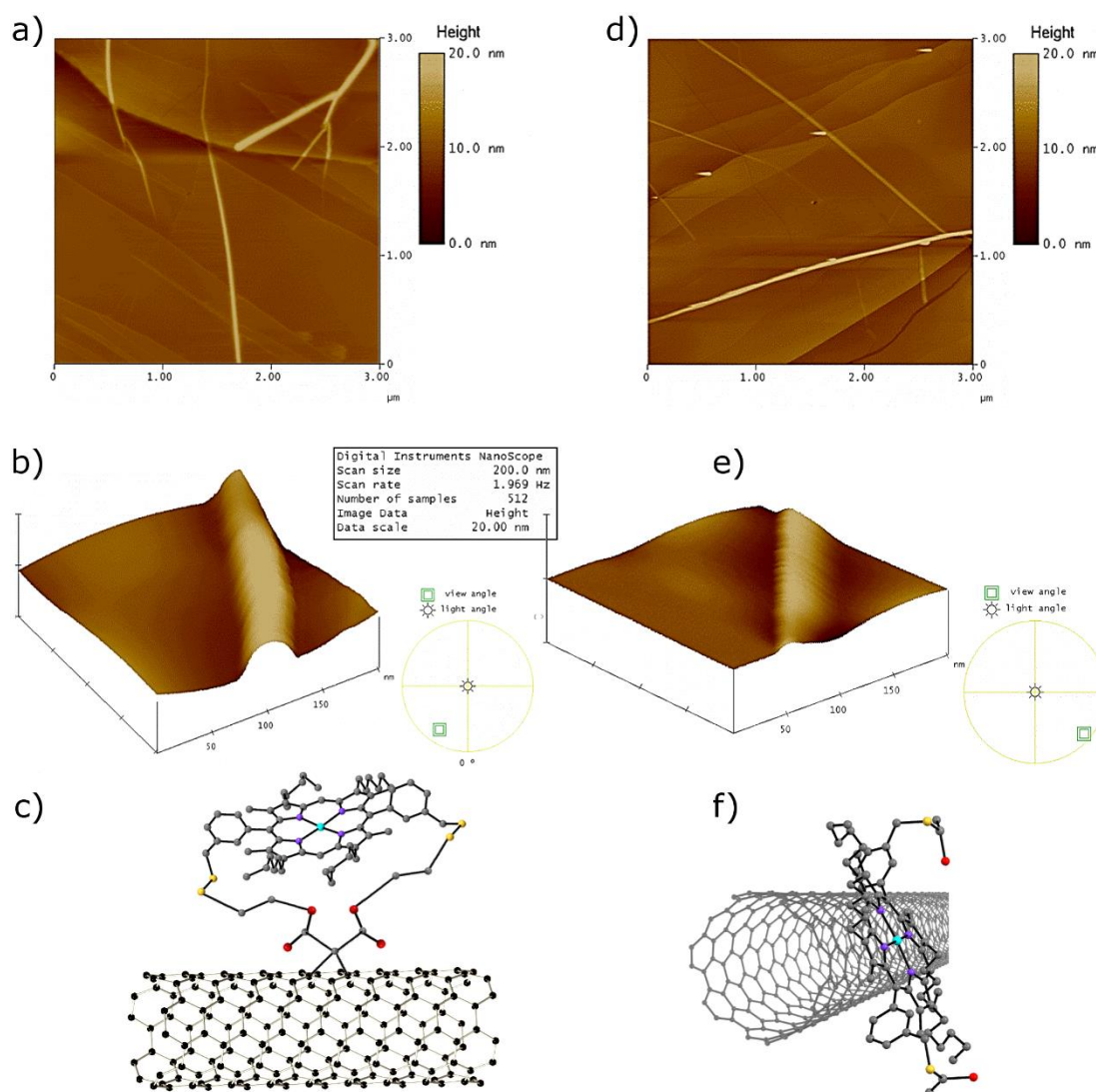


**Figure 5.** Tapping Mode AFM imaging on mica surfaces: (a), (b) image and 3D representation of AFM image of covalent Zn(II)-porphyrin@SWNTs nanohybrids (6); (c) Schematic diagram of compound (6); (d),(e) image and 3D representation of non-covalent Zn(II)-porphyrin@SWNTs nanohybrids (2), (f) Schematic diagram of compound (2)

of the nature of the bond between the two components of the complex (porphyrin and SWNTs) as well as the presence or absence of a linker. This generated a substantial morphologic variation, highlighting the significance of choosing a covalent or supramolecular approach for SWNTs functionalization. Such differences observed in the estimated diameters of the nanohybrids (2) vs (6) could be assigned to the following: *i*) the different surface arrangement of the Zn(II)-porphyrin on the surface of SWNTs in the non-covalently linked complex, *ii*) the plane of the porphyrin containing the four pyrroles rings is parallel to principal axis of the SWNT and *iii*) the aromatic ring stacking interactions maintain the porphyrin linked to the SWNT. Within the covalently linked complex (6), the plane of the porphyrin is likely held at a longer distance with respect to the principal axis of the SWNT, compared to the case of (2). However, the diameter differences observed between the two specimens may also be due to several SWNTs assembled together and thus forming bundles.

TEM measurements were employed to further characterize the morphology of SWNTs. The **Figure 6b** shows TEM micrograph of non-covalent Zn(II)-porphyrin@SWNTs complex (2). Dark areas with stronger contrast arise due to the presence of zinc, while the brightest sites of interest correspond to areas where there are only lighter elements such as hydrogen, carbon and nitrogen, consistent with the EDS analyses of different areas of interest. **Figure 6b** shows that the SWNT have a rough surface likely due to the aggregates formed by porphyrin nanocrystallization. The significant presence of a surface-roughened SWNTs indicates coverage of the surface, suggesting the presence of the Zn(II)-porphyrin on the surface of the SWNTs.<sup>[23]</sup>

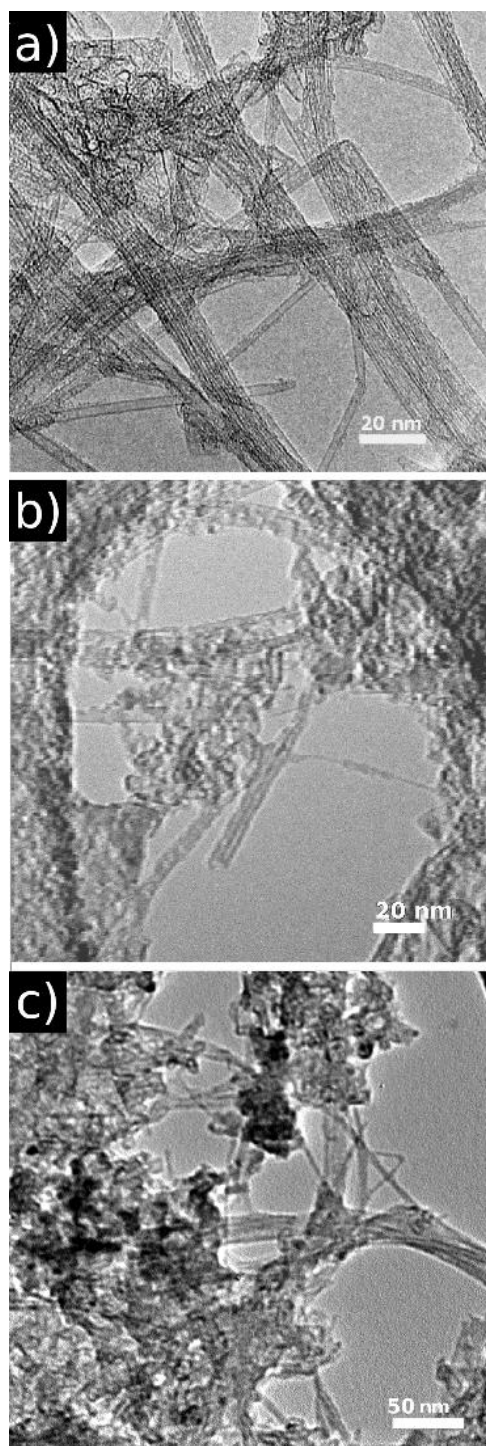


**Figure 6.** TEM microscopy: (a) the free pristine SWNTs; (b) non-covalent Zn(II)-porphyrin@SWNTs nanohybrids (2); (c) covalent Zn(II)-porphyrin@SWNTs nanohybrids (6).

TEM micrograph of the covalent Zn(II)-porphyrin@SWNTs complex (6) (Figure 6 (c)) shows a rather homogenous distribution of the complex over the surface of the SWNTs with regular aggregation points (areas with stronger contrast) and a lower agglomeration of the SWNTs was observed for 6 vs 2. These subtle differences in morphology observed in the micrographs of (2) and (6) might be explained by the covalent bond of the Zn(II) porphyrin to the SWNTs which strongly immobilizes the molecules, reducing their agglomeration and

improving their homogenous distribution over the surface of the SWNTs. In complex (2), the donor-acceptor nature of the non-covalent bond between Zn(II)-porphyrin and SWNTs allows for a higher degree of porphyrin mobility onto the  $sp^2$  surface. Therefore, a non-homogeneous distribution of the donor molecules onto the acceptor surface can facilitate the aggregation of porphyrin molecules. AFM and TEM (both deemed reliable techniques to assess the morphology of materials produced by chemical modification of the surface of SWNTs) confirm the formation of isolated individual SWNT from bundled ropes upon derivatisation.<sup>[22]</sup>

Both covalently and non-covalently linked Zn(II)-porphyrin@SWNTs nanohybrids were found to be relatively well dispersed in organic solvents upon specimen preparation for microscopies. Pristine SWNTs were found to be more difficult to disperse in solution even after prolonged treatment of sonication, and also the intact SWNTs were observed to be aggregated on the Highly Ordered Pyrolytic Graphite (HOPG) substrate. A similar conclusion regarding aggregation behavior can be derived from absorption spectroscopy in the dispersed phase (*vide infra*).

#### Surface derivatization studies on SWNT hybrids by Raman and XRD spectroscopy

Raman spectroscopy was applied to evaluate the bulk properties and probe the degree of crystallinity of graphitic carbon structure, including whether or not this structure remained intact following extensive synthetic chemistry manipulations.<sup>[24]</sup>

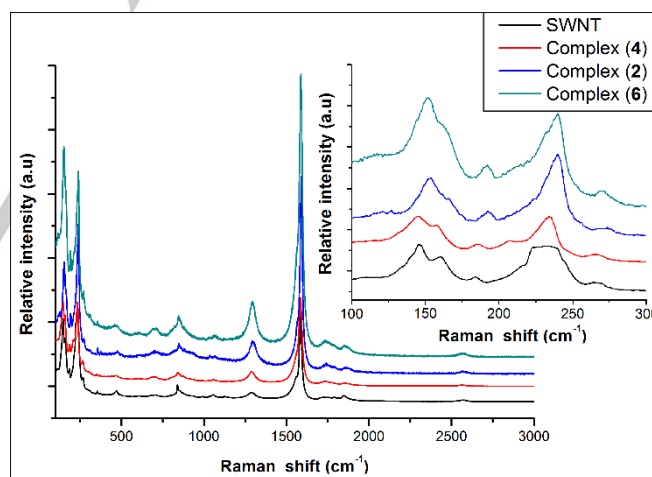


**Figure 7.** Solid state Raman spectroscopy of SWNT (830 nm), Bingel reaction purified SWNT (4), non-covalently linked SWNTs@Zn(II)-porphyrin complex (2) and covalently linked SWNTs@Zn(II)-porphyrin complex (6); Inset: Raman spectrum RBM.

The Raman spectra shown in Figure 7 were recorded by dispersing samples in  $\text{CHCl}_3:\text{EtOH}$  (1:1) using the excitation wavelength  $\lambda_{\text{ex}}$  of 830 nm. Spectra showed the G band at ca  $1581 \text{ cm}^{-1}$  region (primary graphitic mode) corresponding to a splitting of the  $E_{2g}$  stretching mode of graphite, reflecting the presence of  $sp^2$ -hybridized carbons. The Raman spectra of SWNTs (4) exhibit a G-band at  $1585 \text{ cm}^{-1}$  and a D band at  $1289 \text{ cm}^{-1}$ . The  $I_D/I_G$  band intensity ratio of covalent functionalized SWNTs (4) (0.16) increased somewhat compared to the  $I_D/I_G$  band intensity ratio of primitive SWNTs (0.11), indicating that

Bingel reaction introduced surface defects and disordered graphite structures onto the SWNTs. It can be seen that the Raman spectra of complex (2) shows G-band at  $1588\text{ cm}^{-1}$  and D-band at  $1292\text{ cm}^{-1}$ . A 0.17  $I_D/I_G$  band intensity ratio was also observed from the Raman spectra of complex (2). Compared to complex (2), the Raman spectra of the covalent Zn(II)-porphyrin@SWNTs complex (6) exhibits G and D bands at  $1588\text{ cm}^{-1}$  and  $1293\text{ cm}^{-1}$  respectively. Moreover, the  $I_D/I_G$  band intensity ratio slightly increases to 0.19. Compared to the  $I_D/I_G$  band intensity ratio of free SWNTs, the ratio of both complex (2) and complex (6) show an increase, which suggests that a supramolecular interaction between of SWNTs and (1) has occurred. Raman spectroscopy also showed peaks located between  $140\text{ cm}^{-1}$  to  $300\text{ cm}^{-1}$ , which correspond to radial breathing modes (RBM) (Figure 7 inset). The free SWNTs contains tubes with a broad diameter ranging 0.8-1.8 nm, while there are two significant and sharp RBM peaks at  $234\text{ cm}^{-1}$  and  $146\text{ cm}^{-1}$ , which indicate that there are tubes with diameters of

1.02 nm and 1.64 nm. The spectra recorded for the covalently functionalized SWNTs in complex (4) remained largely unchanged with respect to free SWNTs, which exhibits two maxima RBM peaks at  $234\text{ cm}^{-1}$  and  $145\text{ cm}^{-1}$ , suggesting that the diameters of the nanotubes are between 1.02nm and 1.64 nm.<sup>[25]</sup> The non-covalent Zn(II)-porphyrin@SWNTs complex (2) shows a maximum RBM peaks at  $240\text{ cm}^{-1}$  and  $154\text{ cm}^{-1}$ . This indicates that in, dispersions of porphyrin (2) in a mixture of  $\text{CHCl}_3$  : EtOH 1:1 contains tubes with diameters of 0.99 nm and 1.55 nm. The RBM frequencies of (6) ( $240\text{ cm}^{-1}$  and  $152\text{ cm}^{-1}$ ) suggest that carbon nanotubes with a diameter of 0.99 nm and 1.57 nm are mainly present.

To verify the nature of the species adsorbed onto the surface of the SWNTs and the nature of their possible binding modes, XPS measurements were carried out. In particular, the C1s, O1s and N1s core levels were evaluated for both Zn(II)-porphyrin@SWNTs nanohybrids and pristine SWNTs.

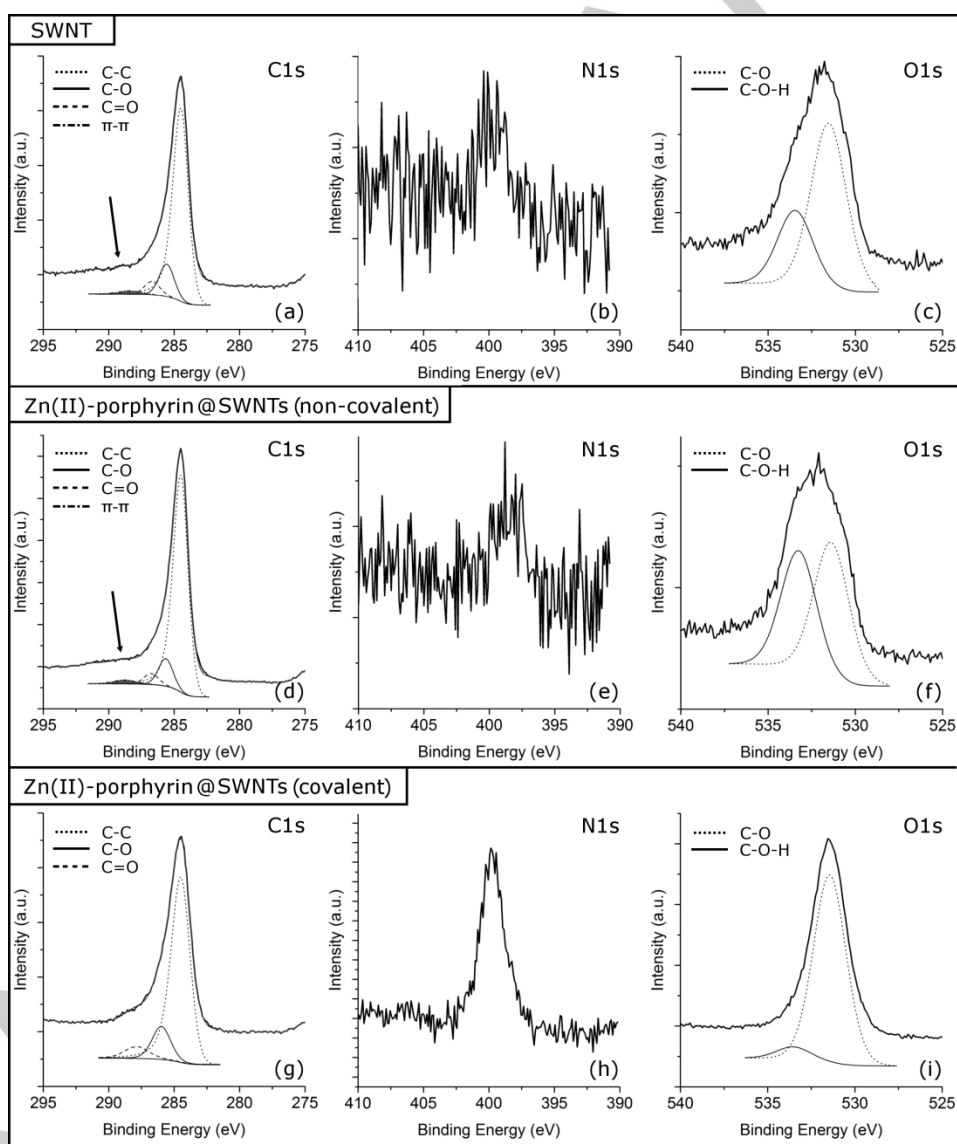


**Figure 8.** XPS spectra corresponding to: (a) C1s region, (b) N1s region, (c) O1s region for the SWNT, (d) C1s region, (e) N1s region, (f) O1s region for the SWNT@Zn(II)-porphyrin (non-covalent), (g) C1s region, (h) N1s region and (i) O1s region for the Zn(II)-porphyrin@SWNT hybrid (covalent).

**Figure 8 (a), (d) and (g)** show the XPS spectra corresponding to the C1s level and, as observed, C-C, C-O and C=O convoluted components can be observed in SWNT and both non-covalent Zn(II)-porphyrin@SWNT (**2**) and covalent Zn(II)-porphyrin@SWNT (**6**) (in SWNT the C-O and C=O signals come from the carbonated surface; in the Zn(II)-porphyrin@SWNT samples they arise from both the carbonates and the CO groups). However, as observed, there is one additional signal in the SWNT and non-covalent Zn(II)-porphyrin@SWNT (**2**) systems, a weak shoulder located at a binding energy slightly above that of the C=O (arrow marked in **Figure 8 (a) and (d)**). This signal can be associated with the existence of  $\pi$ - $\pi$  interactions between the SWNTs and/or the Zn(II)-porphyrins, e.g. non-covalent bonding. The lack of this component in the Zn(II)-porphyrin@SWNT (covalent) suggests that the presence of Zn(II)-porphyrin systems covalently linked to the surface of the SWNTs avoid the  $\pi$ - $\pi$  interactions between the SWNTs. **Figure 8 (b), (e) and (h)** show the XPS spectra corresponding to the N1s core level of the samples. As observed only in the case of the Zn(II)-porphyrin@SWNT (covalent) system can be observed a component at 399.7 eV which can be ascribed to an N-C chemical environment. This is indicative of the presence of Zn(II)-porphyrin@SWNT at the SWNTs surface, as expected. However, the absence of this signal in the spectrum of Zn(II)-porphyrin@SWNT (non-covalent) **Figure 8 (e)** and the similarity between the C1s spectra of pristine SWNTs and Zn(II)-porphyrin@SWNT (non-covalent) can be ascribed to the formation of Zn(II)-porphyrin aggregates and the heterogeneous distribution of the Zn(II)-porphyrin molecules. This last feature is in strong agreement with the TEM and AFM results. Finally, **Figure 8 (c), (f) and (i)** show the O1s spectral decomposition. In all cases C-O and C-O-H convoluted components can be observed, showing that the covalent Zn(II)-porphyrin@SWNT sample have a low presence of C-O-H species at the SWNT surface with respect to the C-O species. On the other hand, the non-covalent Zn(II)-porphyrin@SWNT presents the highest level of this species indicating a more hydroxylated surface of the SWNTs

#### DFT calculations

To understand further the geometry adopted by an isolated Zn(II) porphyrin molecule bound non-covalently onto a single, model, SWNT strand and the nature of its interaction with this aromatic 'guest', DFT calculations using CASTEP<sup>[26]</sup> code were performed. A model fragment of a single strand capped [10,10] nanotube was selected as this is 1.6 nm wide, consistent with the expectations from Raman spectroscopy, and its ability to bind supramolecularly with the porphyrin molecule (**1**) was estimated using a gas phase modelling approach which has been successfully applied in previous studies.<sup>[11c, 27]</sup> One of our previous modelling considered a composite formed between a tripod porphyrin trimer unit and a capped [10,10] SWNT<sup>[11c]</sup> whereby two of the three porphyrin units were found to interact closely with the surface of the SWNT. In that initial model, the binding energy was calculated to be -2.046 eV (-1.023 eV per porphyrin unit) and the charge transfer was estimated to be 0.003 electrons clearly indicating non-covalent nature of the binding. In a related 'host-guest' approach, but involving a different chromophore, a naphthalenediimide molecule was

allowed to bind supramolecularly onto the middle part and tip of a [10,10] capped SWNT and their binding energies were -0.84 eV and -0.66 eV respectively.<sup>[27]</sup>

The magnitude of the binding energy depends on the type of the small molecule involved and the level of theory adopted. The amount of charge transferred in the porphyrin-SWNT model used hereby was calculated to be 0.044 electrons in the tip-binding configuration and 0.086 electrons in the middle-binding configuration again showing the non-covalent interaction. In the model reported hereby, the occurrence of van der Waals (vdW) interactions was considered. As this interaction is attractive, our calculated binding energy is slightly higher as expected. However, calculated binding energies and the amount of charge transferred in the model reported hereby are consistent with our previous models. In literature a very few computational studies are available on single porphyrin units absorbed on SWNTs.<sup>[28]</sup> Basiuk *et al.* have studied the noncovalent functionalization of carbon nanotubes with porphyrin theoretically.<sup>[29]</sup> **Figure 9a** shows the DFT relaxed geometries of model compounds used in this study. It is likely that the aromatic stacking of the porphyrin-SWNTs alters the optical properties of the emerging nanocomposite and ensures the preservation of a non-covalent monomeric porphyrin unit ready for a controlled donor-acceptor interlayer association with SWNTs. From the dimer structure determinations by synchrotron single-crystal X-ray diffraction, it can be seen that the size of the Zn(II)-porphyrin measured between the methyl groups of the phenyl rings is 16.55 Å. This value is larger than the calculated inner space for [8,8], [9,9] and [10,10] SWNTs (**Figure 9d**). Therefore, all of the porphyrin molecules will bind to the outside of the SWNTs and interact with their outer surface.

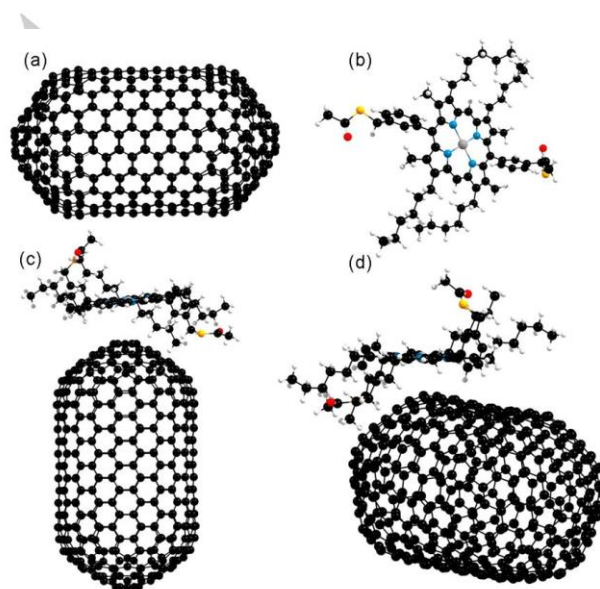


**Figure 9 a)** DFT optimized structures of model compounds: a short [10,10] capped SWNT; **b)** Zinc (II) centered porphyrin molecule; **c)** porphyrin molecule bound supramolecularly onto the tip of a [10,10] capped SWNT (configuration **A**); **d)** porphyrin molecule bound supramolecularly onto the middle part of a [10,10] capped SWNT (configuration **B**). (black-carbon, red- oxygen, blue-nitrogen, yellow-sulphur, white-hydrogen, zinc-grey).

The calculated binding energies for the porphyrin molecule interaction with the tip of the SWNT (configuration **A**) and the sidewall of the SWNT (configuration **B**) are  $-0.69$  eV and  $-1.55$  eV respectively, indicating a  $\pi$ -orbital interaction between the porphyrin molecule and SWNT. The negative values of binding energies indicate that both complexes are thermodynamically stable. Total energies calculated for each systems and the methodology we adopted to calculate the binding energy are given in the supplementary information. Mulliken population charge analysis was carried out to estimate the charge transfer between porphyrin and SWNT. Calculations showed that for a model composite with configuration **A** (tip-binding geometry), 0.04 electrons were transferred between a molecule of porphyrin and the [10,10] SWNT. For the configuration **B** (where a porphyrin molecule is bound to the middle of the SWNT), 0.08 electrons were transferred locally between one porphyrin unit and the small model of a carbon nanotube considered.

The DFT-relaxed model used for computational studies considered only a very short length for the SWNT modelled (200 nm): this allows a maximum of four porphyrin molecules to bind configuration **A** (coating the tip of the SWNTs) and a further 6 porphyrin molecules to bind in configuration **B** (to the middle part of the SWNT). This DFT gas-phase modelling estimates approximately 2 electrons are transferred between 10 molecules of porphyrin absorbed onto the outer surface of a 500 nm length of capped SWNT fragment. This electron transfer can be attributed to the donor-acceptor interaction between a porphyrin molecule and SWNT. DFT calculations were employed to obtain a direct view of the equilibrium geometry and the electronic structures for the frontier orbitals of the Zn(II)-porphyrins. The crystal structures of the above complexes were used as an input geometry for gas phase optimization by B3LYP 6-31G(d,p), whereby a restricted spin was used for the optimization of the diamagnetic zinc(II) porphyrin complex.

The calculated electronic structures did not show negative frequencies, indicating that the optimized geometries are in the inclusive energy minima.<sup>[30]</sup> Porphyrins with  $D_{4h}$  symmetry generally show energetically degenerate two lowest unoccupied molecular orbitals (LUMO+1, LUMO) and nearly degenerate two highest occupied molecular orbitals (HOMO, HOMO-1), as shown in **Figure 10**. **Table S3** (ESI) shows the energy level of each molecular orbital. The calculated energy band gap for Zn(II)-porphyrin was 3 eV, which indicates the visible light absorption behavior, and promising potential photovoltaic properties can be applied in the design of solar cells. Such energy gap appears is in accordance with results recently reported for Zn(II)-porphyrin species.<sup>[31]</sup> Together with the molecular orbital structure and the calculated energy level, it can be found that after modification at both *meso*-positions and  $\beta$ -positions with aryl thioacetate-functionalized side groups and hexyl chains respectively, the rich electron density areas were moved from the macrocyclic ring (shown in HOMO) center to *meso*-positions (as shown in LUMO) and  $\beta$ -positions (as shown in LUMO+1). These results show that the substitutions onto *meso*-positions and  $\beta$ -positions of Zn(II)-porphyrin mainly affect the energy levels for unoccupied orbitals of the Zn(II)-porphyrin. Since these molecular orbitals are involved in the ligand (including the phenyl substituent) and the metal it is highly likely that both contribute to the UV-vis light absorption properties.

This observation may explain the observed similarity between the UV-vis absorption bands in this family of

compounds as well as the small metal dependency. Modelling results also explain the observation that the substitutions of the side groups and hexyl chains may play a dominant role in determining fast electron injection from the excited singlet state of Zn(II)-porphyrin to other coordinate materials such as carbon nanotubes, graphene oxide or reduced graphene oxide. Such interactions may be of relevance in the current quest for new sustainable chemistries approaches to enhance the performances of solar cells and bio-sensing devices.

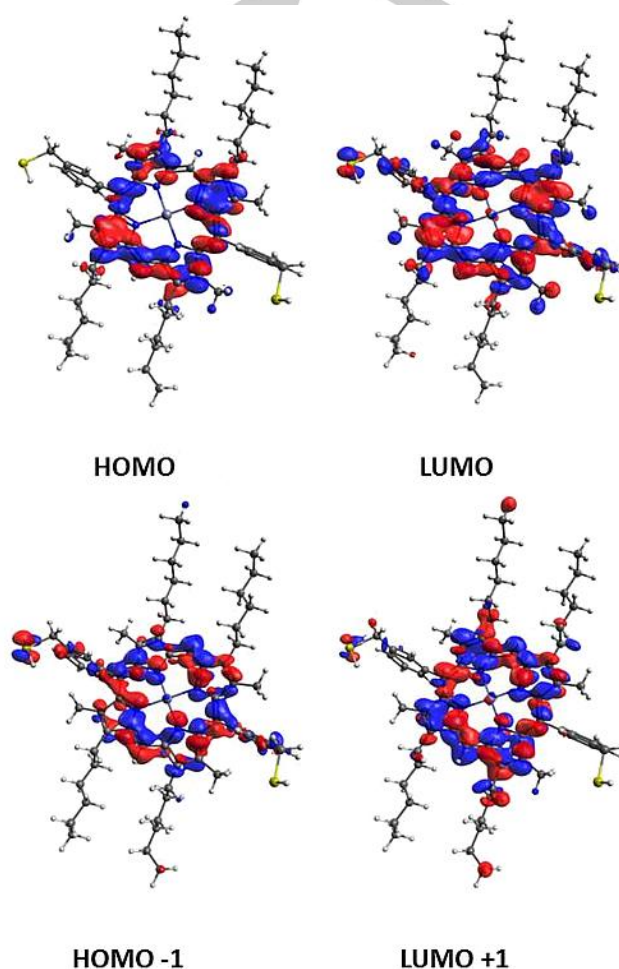


**Figure 10.** a) Two highest occupied and lowest unoccupied molecular orbital of de-protected Zn(II)-porphyrin (**3**) from gas phase DFT calculations

UV-vis spectroscopy was carried out to further investigate the optical absorption behavior of nanocomposites (**2**) and (**6**) in dispersed phases. The supramolecular assembly of Zn(II)-porphyrin and SWNTs was studied by using optical spectroscopy (**Figure 50** and corresponding experimental details, ESI). **Figures S51a-b** (ESI) exhibit the UV-vis absorption spectra of Zn(II)-porphyrin dispersed in 1:1 o-DCB and chloroform (3 mL, 1  $\mu$ M) and titrated with a dispersed mixture of Zn(II)-porphyrin (**1**) (0.5  $\mu$ M) and SWNTs in 1:1 orthodichlorobenzene (o-DCB) and chloroform suspensions.

**Figure 11** shows the optical absorption spectra of Zn(II)-porphyrin, SWNTs, non-covalent Zn(II)-porphyrin@SWNTs complex (**2**) and covalent Zn(II)-porphyrin@SWNTs complex (**6**). Zn(II)-porphyrin (**1**) shows a main absorption peak at 417 nm, while the intact SWNTs do not show any obvious absorption

band in UV-vis spectral range. After the SWNTs are covalently linked to Zn(II)-porphyrin, the complex (**6**) show a peak at 420 nm, slightly red shifted compare with the intact Zn(II)-porphyrin (**1**). The Zn(II)-porphyrin@SWNTs (non-covalent) complex (**2**) shows a red-shifted main absorption peak at 436 nm. These results suggest that the chromatic shift of complex (**2**) and complex (**6**) is due to the nature of the interaction of Zn(II)-porphyrin with the SWNTs. The covalent interaction between SWNTs and Zn(II)-porphyrin seems to minimize the extent of the red shift observed. The UV-vis-NIR spectra of Zn(II)-porphyrin@SWNT (recorded in pure CHCl<sub>3</sub>) shows the typical S<sub>22</sub> transitions, in the region around 960 nm. Partially overlapping of S<sub>22</sub> and metallic M<sub>11</sub> transitions characteristic to SWNTs can be seen at 500-1000 nm in Zn(II)-porphyrin@SWNT. Since the transition energies are related to the size of the SWNT bundles and the presence of isolated tubes in solution have been reported to give rise to sharp, well-resolved peaks,<sup>[27]</sup> UV-vis-NIR spectroscopy of the Zn(II)-porphyrin@SWNT composite suggests that Zn(II)-porphyrins are capable of efficient attachment onto the surface of SWNTs. Due to the enhanced dispersibility caused by the attachment of Zn(II)-porphyrin, this absorbance band may well constitute a further indication of the de-bundling of the SWNT strands in solution.

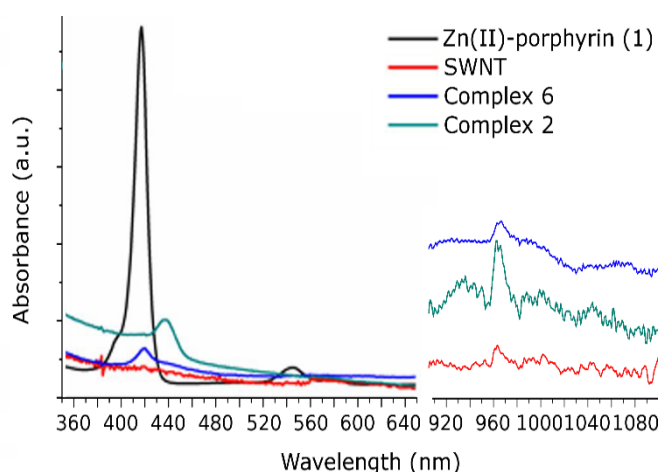


**Figure 11.** UV-vis and UV-Vis-NIR spectroscopy of Zn(II)-porphyrin, intact SWNTs, non-covalent Zn(II)-porphyrin@SWNTs nanohybrids (**2**) and covalent Zn(II)-porphyrin@SWNTs nanohybrids (**6**).

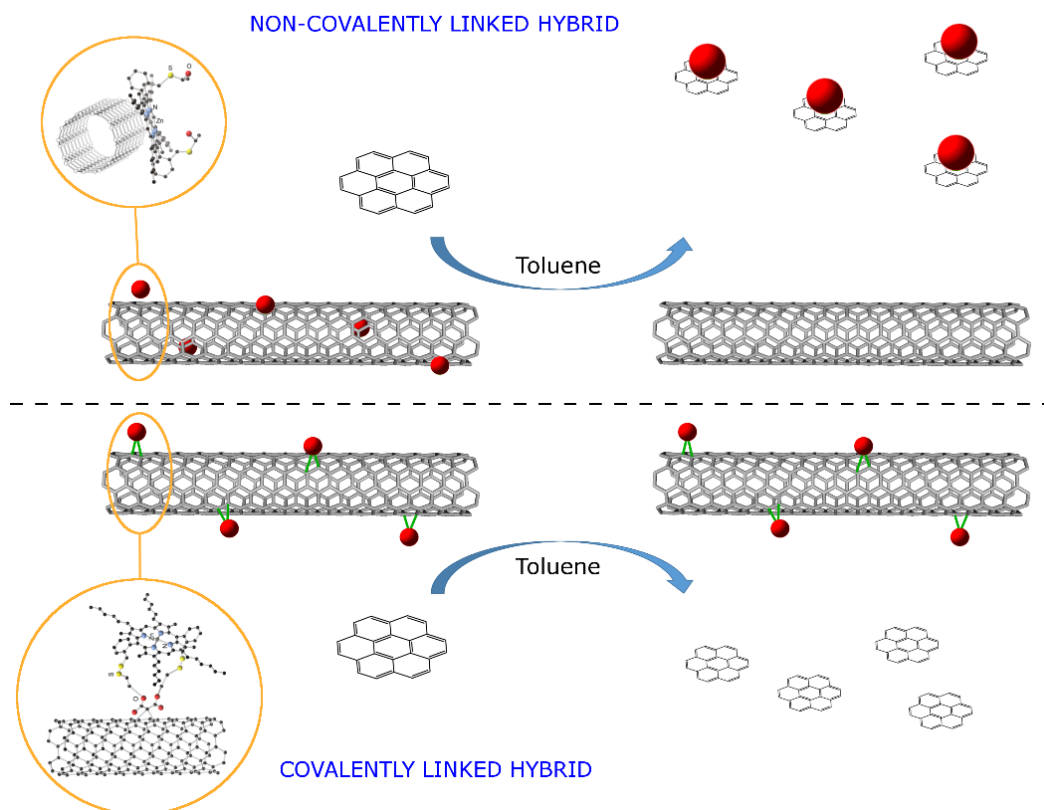
The extent of a supramolecular interaction between aromatic molecules and carbon nanostructures has been previously studied by using a smaller fraction of a sp<sup>2</sup> carbon system.<sup>[32]</sup> To demonstrate how the covalently and non-covalently linking strategies may differ in their effectiveness to connect the porphyrins with SWNTs, a small aromatic competitor molecule, coronene, was introduced in suspensions of covalent and non-covalent Zn(II)-porphyrin systems (**2**) and (**6**). This was expected to induce the dissociation of the donor-acceptor complexes and to allow the monitoring of this process in the dispersed phase by absorbance spectroscopies. While the high affinity (binding constant) of coronene for the Zn(II)-porphyrin molecules induce a competitive equilibrium that facilitates the dissociation of the non-covalent Zn(II)-porphyrin@SWNTs system and the formation of a new Zn(II)-porphyrin @coronene

complex, this type of complex cannot be generated when Zn(II)-porphyrin molecules are covalently attached to the surface of the SWNTs. Coronene was chosen deliberately as the competitor molecule as it can act as a simple model for the larger carbon-based materials whilst providing an insight into the possible  $\pi$ - $\pi$  interactions between porphyrin and carbon single-walled nanotubes. It would also facilitate the evaluation of the degree of supramolecular aggregation (**Scheme 1**). Data fitting involved a 1 : 1 binding isotherm model and the association constant, K<sub>1:1</sub>, was estimated to be 4.62 x 10<sup>4</sup> M<sup>-1</sup> (ESI). Therefore, coronene is indeed capable of acting as a competitive candidate likely to disrupt the interactions between the SWNTs and Zn(II)-porphyrin systems (**Scheme 1**).

A recent report<sup>[12]</sup> described the complexity of the non-covalent interactions between aromatic electron-poor molecules, such as functional naphthalenediimides (NDI), and planar carbon-based materials such as thermally reduced graphene oxide (TRGO), as well as the use of coronene to elucidate the intimate nature of the donor-acceptor system, but, to the best of our knowledge such competitive experiment involving functional zinc porphyrins and SWNTs has not been reported on thus far.

#### *Fluorescence spectroscopy in solution and fluorescence lifetime imaging microscopy (FLIM) on thin film*

To investigate the fluorescence emission behavior of Zn(II)-porphyrin upon covalent and non-covalent SWNTs linked complexes, two-dimensional fluorescence spectroscopy was performed. 2D fluorescence contour plotting of free Zn(II)-porphyrin, SWNTs, non-covalent Zn(II)-porphyrin@SWNTs complex (**2**) and covalent Zn(II)-porphyrin@SWNTs complex (**6**) were carried out in a 200- 800 nm excitation-emission range. Free Zn(II)-porphyrin (**1**) shows a strong emission peak between 570 nm and 670 nm (**Figure 12a**). A strong Rayleigh scattering line is shown in the two-dimensional contour plot of SWNTs (**Figure 12b**), but no detectable fluorescence emissions is observed from the SWNTs suspension. After porphyrin (**1**) was non-covalently linked to the SWNTs surface via  $\pi$ - $\pi$  stacking, the excitation-emission, observed for a Zn(II)-porphyrin (**1**) solution, was remarkably quenched. Moreover, a blue shift of emission maximum wavelength can be observed from 570-670 nm to 530-610 nm (**Figure 12c**). Such quenching behavior and associate blue shifting (from 570-670 nm to 520-590 nm) can also be found in the two-dimensional fluorescence spectra of the covalently linked complex (**6**) (**Figure 12d**). The intensity of the emission maximum for the covalently linked was observed to slightly decrease in comparison to the non-covalently linked complex. The fluorescence quenching of emission maximum wavelength indicates that an energy transfer process from the Zn(II)-porphyrin to the SWNTs has occurred, while the blue shift is generated due to the non-covalent interaction of porphyrin with the carbon surface. These results confirm the non-covalent adsorption interaction between Zn(II)-porphyrin and SWNTs and, at the same time, the covalent nature of the porphyrin-SWNTs bond in the nanohybrid (**6**).



**Scheme 1.** Addition of coronene (1  $\mu\text{M}$  solution in toluene) and washing process of the suspensions of the non-covalent and covalent nano hybrids Zn(II)-porphyrin@SWNTs (**2**) and (**6**) in 1:1 toluene : chloroform.

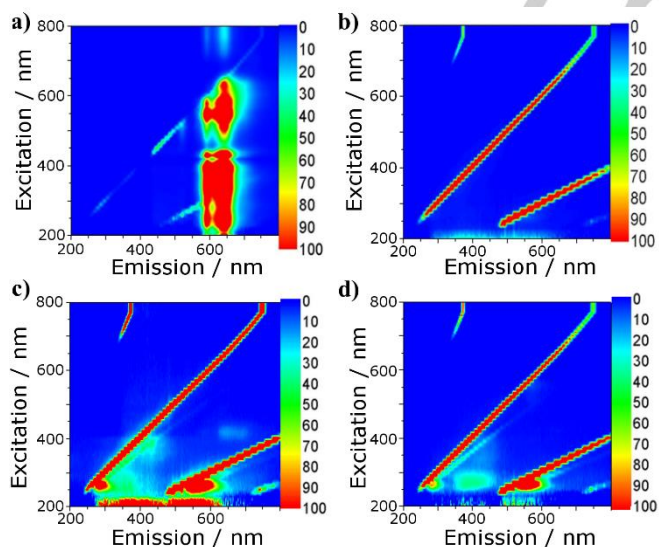


**Figure 12.** Two-dimensional fluorescence contour plotting of (a) Zn(II)-porphyrin, 1  $\mu\text{M}$  (1:1 ethanol : chloroform); (b) SWNT, 0.5 mg/mL (1:1 ethanol : chloroform); (c) non-covalent Zn(II)-porphyrin@SWNTs complex (**2**), 1 mg/mL (1:1 ethanol : chloroform) and (d) Zn(II)-porphyrin@SWNTs (covalent) complex (**6**), 1 mg/mL (1:1 ethanol : chloroform).

Time correlated single photon counting measurements were carried out in order to further investigate the excited state characteristics of Zn(II)-porphyrin (Table 1 and Figure S46 in ESI). In solution studies, the TCSPC fluorescence decay data of compound **1** (2-photon excitation at 810 nm) shows the presence of major component with short lifetime decay ( $a_1 = 93.2\%$ ,  $t_1 = 39$  picoseconds) and minor longer lived component ( $a = 6.8\%$ ,  $t_2 = 1483$  picoseconds, Table 1).

**Table 1.** Time-Correlated Single Photon Counting (TCSPC) (2 photon excitation,  $\lambda_{\text{ex}} = 810$  nm) of Zn(II)-porphyrin 1  $\mu\text{M}$  in DMF:Toluene. Laser power was 5.4 mW.

	$\chi^2$	$\tau_1(\text{ps})$	$a_1(\%)$	$\tau_2(\text{ps})$	$a_2(\%)$	$\tau_m(\text{ps})$
1	1.50	$39 \pm 5.0$	93.2	$1483.5 \pm 2.8$	6.8	136.67

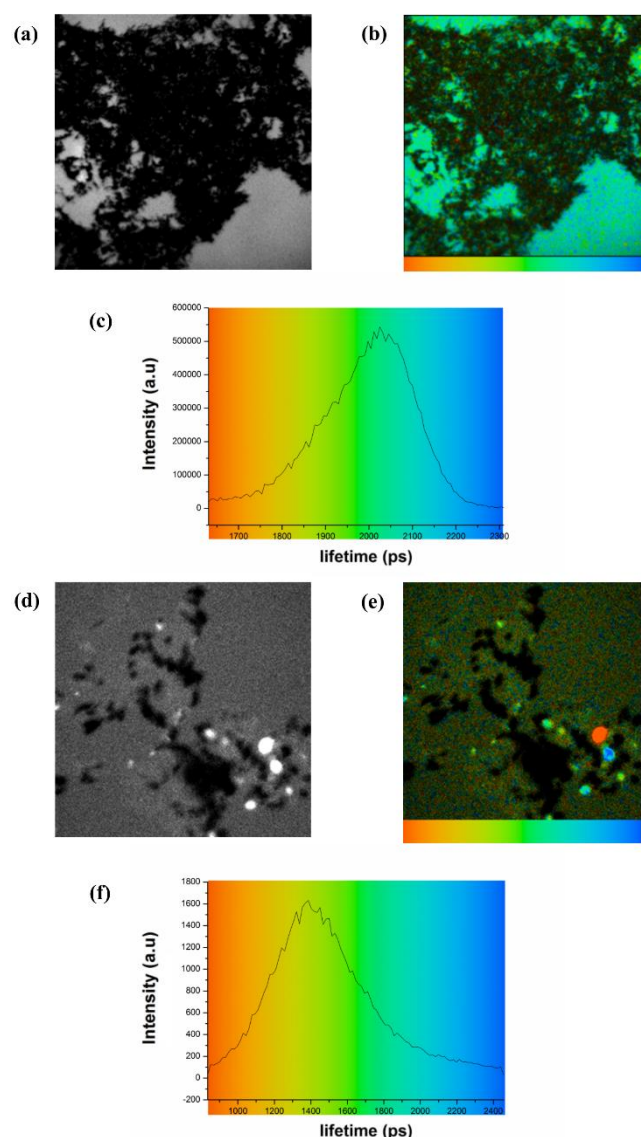


**Figure 13.** Single-photon fluorescence lifetime map ( $\lambda_{\text{ex}} = 473$  nm) and corresponding intensity images of: (a and b) solid non-covalent Zn(II)-porphyrin@SWNTs complex (2) and corresponding lifetime distribution curve (c); solid covalent Zn(II)-porphyrin@SWNTs (6) complex (d and e) and corresponding lifetime distribution curve (f). (b and e). Images a and d represent intensity images on thin films. A color coded bar is provided for direct correlation between the lifetime colour map (b and e) and lifetime histograms (c and f).

**Table 2.** Solid state FLIM data for free base porphyrin precursor (denoted Prec. in table), Zn(II)-porphyrin (1), (non-covalent) Zn(II)-porphyrin@SWNTs complex (2) and (covalent) Zn(II)-porphyrin@SWNTs complex (6).

	$\chi^2$	a1(%)	$\tau_1$ (ps)	a2(%)	$\tau_2$ (ps)	$\tau_m$ (ps)
Prec.	1.3	84.1	244±26.0	15.9	3369.7±460.1	742.0±155.9
1	1.17	87.3	554±55.0	12.7	1715.6±231.6	765.3±96.6
2	1.49	98.8	35±4.5	1.2	870.8±75.1	44.9±6.1
6	1.15	98.7	28±11.8	1.3	6880.1±228.0	120.5±67.1

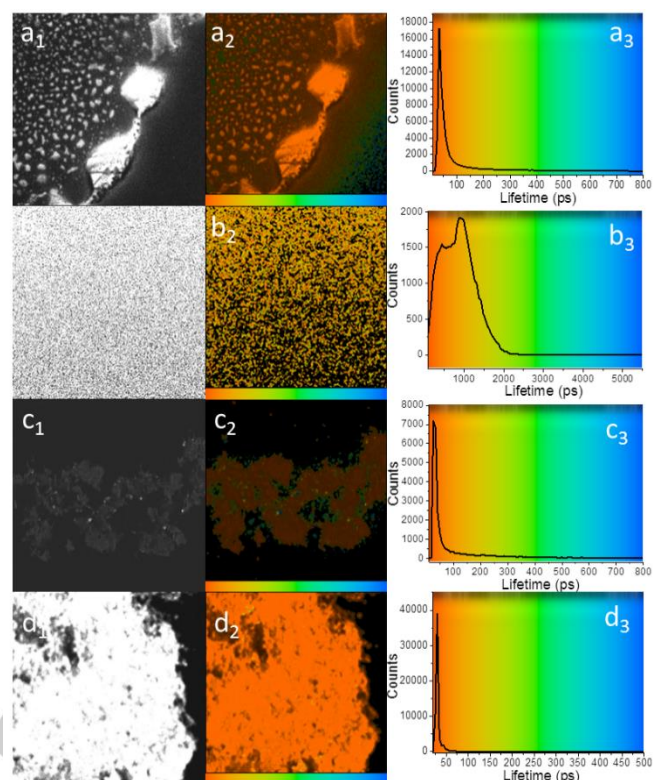


**Figure 14.** Two-photon fluorescence lifetime map ( $\lambda_{\text{ex}} = 810$  nm) of microcrystalline free base porphyrin (a<sub>1</sub>; a<sub>2</sub>) and associate lifetime profile distribution across the image (a<sub>3</sub>); microcrystalline Zn(II)-porphyrin complex (b<sub>1</sub> and b<sub>2</sub>), and associate lifetime profile distribution (b<sub>3</sub>); non-covalent solid Zn(II)-porphyrin@SWNTs complex (2) (c<sub>1</sub> and c<sub>2</sub>), and corresponding lifetime distribution curve c<sub>3</sub>; solid covalent Zn(II)-porphyrin@SWNTs complex (6) (d<sub>1</sub> and d<sub>2</sub>) and corresponding lifetime distribution curve (d<sub>3</sub>). Images: a<sub>1</sub>, b<sub>1</sub>, c<sub>1</sub> and d<sub>1</sub> are two photon intensity images. A color coded bar is provided for direct correlation between the lifetime colour maps a<sub>2</sub>, b<sub>2</sub>, c<sub>2</sub> and d<sub>2</sub> and lifetime histograms (a<sub>3</sub>, b<sub>3</sub>, c<sub>3</sub>, d<sub>3</sub>), respectively.

The interactions and consequent energy transfer between SWNTs and Zn(II)-porphyrin were further investigated using laser induced single-photon excitation and fluorescence emission excited state lifetime measurements. When in solid state, the fluorescence decay of Zn(II)-porphyrin@SWNTs could be fitted to a single component with a single lifetime of approximately 2000±100 ps following excitation at 473 nm (Figure 13a and 13 b). An additional relatively broad maximum in the lifetime distribution curve (Figure 13c) was also observed. Such broad full width at half of the maximum (FWHM) suggests the presence of a heterogeneous fluorescence decay population and also confirmed the formation of various crystalline supramolecular assemblies and hybrid structures. Figures 13d and 13e show lifetime emission maps of solid-state covalent Zn(II)-porphyrin@SWNTs complex (6) using similar conditions to the measurement carried out for non-covalently linked complex (2). Shown in Figure 13f, the corresponding lifetime distribution curve proved a shorter lifetime measured in complex (6), 1400±100 ps. A broad FWHM of the corresponding lifetime distribution curve was also observed. The difference in major lifetime between the covalent complex (6) and non-covalent complex (2) also indicates the two types of synthesis strategies

result in different electronic interactions between the Zn(II)-porphyrin and the SWNTs and different degrees of quenching.

To further investigate the role of SWNT as a quencher of zinc and free base porphyrins, two-photon FLIM for free-base porphyrin and Zn(II)-porphyrin, as well as solid complexes (**2**) and (**6**) were carried out (Figure 14a-d). For such measurements, two component systems ( $\tau_1$  and  $\tau_2$ ) were more accurate models of the decay profiles (Table 2 and Figure S38-S41, see in ESI). Micro-crystallites of free base porphyrin and Zn(II)-porphyrin (**1**) imaged on borosilicate glass showed similar fluorescence decay profiles with  $\tau_m$  (average lifetime) of  $742 \pm 155.9$  and  $765 \pm 96.6$  picoseconds respectively. Interestingly, the major component for the non-covalent Zn(II)-porphyrin@SWNTs complex (**2**) was significantly reduced (from  $554 \pm 55.0$  to  $35 \pm 4.5$  picoseconds). The same shortening in lifetime for the first component of the covalent complex (**6**) can be seen. In this instance, however, the extent of shortening is even more pronounced. In agreement with what observed for the single-photon excitation mechanism, the covalent functionalization of SWNTs results in a more significant lifetime shortening. The appearance of a second longer minor component suggests instead the presence of unquenched species free in solid state (free based or zinc porphyrins) or their supramolecular self-assembled structures.<sup>[12]</sup>

We have recently reported that these changes in lifetime upon complexation, particularly the presence of a lower lifetime component may account for a photo-induced excited state energy transfer occurring between the closely bound donor-acceptor systems aromatic chromophores and planar carbon based materials.<sup>[12]</sup> Therefore, it is reasonable to conclude that a Förster Resonance Energy Transfer (FRET) occurs in these systems, where the porphyrins act as FRET donors and the SWNTs as the corresponding FRET acceptor.<sup>[12, 33]</sup>

## Conclusions

A multi-pronged characterization protocol involving imaging and spectroscopy methodologies probed the supramolecular properties of a Zinc(II) substituted bulky aryl porphyrin. This tailored Zn(II)-porphyrin synthon and pristine SWNTs were used as building blocks leading to new Zn(II)-porphyrin@SWNTs adducts which were either covalently or non-covalently linked. The new nanocomposites materials have been synthesized by following either supramolecular self-assembly via  $\pi$ - $\pi$  stacking or via a disulfide linker bridging covalently the two components. The morphology and photochemical behavior were thoroughly analyzed by AFM, STED, TEM, Raman, XPS, fluorescence spectroscopies including two-photon excitation spectroscopies. Experiments showed that the Zn(II)-porphyrin functionalization is uniform and the two linking strategies also led to different morphologic characteristics for the functionalized SWNTs, as observed by AFM. The DFT calculations confirmed that the Zn(II)-porphyrin of choice and its carbon monohybrids show potential to be applied in photovoltaics or and bio-sensing devices. For the first time, XPS was used to evaluate the presence of  $\pi$ - $\pi$  interactions as an evidence of non-covalent interaction between the porphyrin and the SWNT. UV-vis, fluorescence spectroscopy and multi-photon confocal fluorescence imaging were carried out to shed light into the nature of the interactions between the porphyrins and SWNTs scaffolds both in solution and in the solid state. The UV-visible studies confirmed the different synthesis strategies produced different light absorption properties. The fluorescence quenching and fluorescence lifetime suggests that a FRET mechanism between the Zn(II)-porphyrin self-assembled tubular aggregates (viewed as the FRET donor) and the SWNTs (FRET acceptor)

occurs in the excited state. The donor-acceptor system designed hereby is predicted to show possible applications in the construction of novel optoelectronic devices using SWNTs as an electron acceptor. Interestingly, the non-covalent linking strategies could help mediate the absorption and emission properties of the original porphyrin. New kinetically stable complex systems emerged and this property is crucial for biosensing applications. The directed, covalent linking strategy provided a strong and stable method to link small molecule and SWNTs whereas in the case of the non-covalently linked strategy, albeit very convenient and rapid, the porphyrin coating is detachable in the presence of other flat aromatic organic molecules capable of acting as competitors. This represents a challenge, as well as an opportunity in designing functional nanohybrids for future sensing applications.

## Experimental Section

**Synthesis of Zn(II)-porphyrin@SWNTs (non-covalent) complex (**2**):** 5 mg purified single-walled carbon nanotubes were added to 30 mL of ethanol. The mixture was sonication for 10 min, three times with 5 min intervals, to make sure majority of the purified SWNTs were dispersed in the solution. The suspension was added to a 50 mL centrifuge tubes and centrifugation at 3500 rpm for 30 min. The top layer supernatant was carefully separated and collected to afford a SWNTs ethanol solution. Afterwards, 1 mg Zn(II)-porphyrin was added to 30 mL of chloroform and the solution added to the SWNTs solution. The mixture was left stirring for 24 hours at room temperature. The mixture was filtrated using a membrane and the solids were rinsed with excess chloroform. The solid nanohybrids were collected and fully dried over 60 °C overnight.

**Bingel reaction for functionalized SWNTs:** For a typical reaction, 30 mg of purified single-walled carbon nanotubes were weighted out and transferred to a quartz tube. The single-wall carbon nanotubes were annealed using a furnace under vacuum at  $10^{-3}$  mbar at 1000 °C for 3 hours under nitrogen protection. The annealing repaired single-wall carbon nanotubes were added to 15 mL dry ortho-dichlorobenzene (o-DCB) to obtain a suspension. A 15 min ultrasonic treatment in 80W sonication bath was introduced to disperse the SWNTs. Afterwards, 1.8 mmol of diethyl bromomalonate and 3.3 mmol of 1,8-diazabicyclo[5.4.0]undecene (DBU) were added to carbon nanotube suspension and the mixture was left stirring for 15 hours under nitrogen protection at room temperature, followed by adding 3.9 mmol trifluoroacetic acid to quench the reaction. 35 mL ethanol was added to the mixture and then the mixture was transferred to a 50 mL centrifuge tube. The mixture was centrifuged at 3500 rpm for 30 min to separate the solvent and single-walled carbon nanotubes. The pellet of SWNTs was washed several times with ethanol by repeating this centrifugation progress. The SWNTs was then collected by a nano-filtrate system and rinsed with more excess ethanol to fully remove the organic phase. The sample was dried at 60 °C overnight.

**Thiol -SH deprotection of Zn(II)-porphyrin:** 3 mg Zn(II)-porphyrin was dissolved in degassed 5 mL  $\text{CH}_2\text{Cl}_2$ , then 200  $\mu\text{L}$  hydrazine monohydrate was added to this mixture. This solution was stirred under nitrogen overnight and the solvent removed under reduced pressure. The product was re-dissolved in degassed 10 mL  $\text{CH}_2\text{Cl}_2$  and washed twice with 20 mL degassed water under nitrogen. The organic phase was dried over sodium sulphate and the solvent was removed by reduced pressure to afford SH- de-protected Zn(II)-porphyrin.

**Synthesis of Zn(II)-porphyrin@SWNTs (covalent) complex (**6**):** Bingel reaction functionalized single-walled carbon nanotubes were trans-esterified by prolonged stirring in an extensive of 2-mercaptoethanol (5 mL) for 72 hours under nitrogen protection. Afterwards, the products  $[(\text{COOCH}_2\text{SH})_2\text{C} < \text{SWNTs}]$  were washed with extensive diethyl ether (80 ml). The mixture was separated by filtration and the solid parts on the filtrate membrane and collected into a glass vial. 1 mg trans-esterified single-walled carbon nanotubes were added to a 5mM chloroform

## FULL PAPER

WILEY-VCH

solution of SH- de-protected porphyrins and then 0.2 % conc. solution containing one equivalent of DBU was added into the mixture drop wise. The solution was stirred for 72 hours at room temperature under nitrogen protection. Afterwards, the mixture was filtrated and the solids on the membrane were rinsed with excess ethanol. The complex was collected and transferred to a 30 mL glass vial. The resulting nanohybrid (black powder) was dried at 60 °C overnight.

**Density Functional Theory (DFT) Calculations:** The calculations to study the equilibrium geometry and electronic structures for the frontier orbitals of the Zn(II)-porphyrins were first performed using density functional theory (DFT) as employed in Gaussian09, using B3LYP 6-31G(d,p).<sup>[34]</sup> This was carried out via the High Performance Computing Facility, Aquila, University of Bath. In order to determine the structure of the complex formed and the nature of the interaction between the Zn(II)-porphyrin and a carbon nanotube, DFT calculations were performed using CASTEP code,<sup>[26]</sup> which solves the standard Kohn-Sham (KS) equations using plane wave basis sets. For the exchange correlation term the Generalized Gradient Approximation (GGA) in the Perdew-Burke-Ernzerhof (PBE) parameterization was employed.<sup>[35]</sup> Ultrasoft pseudopotentials were generated using the “on the fly” formalism in CASTEP. A plane wave basis set with the energy cut-off of 500 eV was used to expand the wave function. As the inclusion of van der Waals (vdW) interactions can improve the binding energy, in this work we have applied vdW corrections as implemented by Grimme<sup>[36]</sup> in the CASTEP package. Structure optimizations were performed using BFGS algorithm and the forces on the atoms were obtained from the Hellman-Feynman theorem including Pulay corrections. In all optimised structures, forces on the atoms were smaller than 0.05 eV/Å and the stress tensor was less than 0.01 GPa. In all calculations, we used super cells with 40 Å, 40 Å and 40 Å vacuum spaces along x, y and z directions respectively. This modelling method makes sure that the nanotubes plus functional groups do not interact with their periodic images. A single k point ( $\Gamma$ ) was used in all calculations.

**Crystal structure determination:** Crystals of Zn(II)-porphyrin dimer were grown from  $\text{CHCl}_3$  and MeOH mixtures. Crystal and structure refinement data are summarized in Table S1 (SI). Data were collected at 180 K on a Nonius Kappa CCD with graphite-monochromated Mo- $K_\alpha$  radiation ( $\lambda = 0.71073$  Å). Also, measurements on the same compound were performed at the synchrotron radiation source at Station 9.8, Daresbury SRS, UK, on a Bruker SMART CCD diffractometer (Wavelength=0.69040) which provided a higher quality data set. In both cases, the same cellular parameters were obtained and the structures were solved by direct methods using the program SIR92.<sup>[37]</sup> The refinement and graphical calculations were performed on the synchrotron data set using the CRYSTALS<sup>[38]</sup> and CAMERON software packages. The structures were refined by full-matrix least-squares procedure on  $F$ . All non-hydrogen atoms were refined with anisotropic displacement parameters. Hydrogen atoms were located in Fourier maps and their positions adjusted geometrically (after each cycle of refinement) with isotropic thermal parameters. Chebyshev weighting schemes and empirical absorption corrections were applied.<sup>[39]</sup>

**Synchrotron crystal data:** C124 H156 N8 S4 Zn2 M = 2017.59, Z = 4, orthorhombic, space group Pbc<sub>a</sub>; a=17.629(5) Å b=17.624(5) Å c=34.458(5) Å  $\alpha = \beta = \gamma = 90^\circ$ ; V=10706(5) Å<sup>3</sup>; T = 150(2) K,  $\mu = 0.535$  mm<sup>-1</sup> Of 31004 reflections measured, 6174 were independent (R<sub>int</sub> = 0.047). Final R = 0.1587 (20768 reflections with I > 3 $\sigma$ (I)) and wR = 0.1892.

[CCDC 1475150 contains the supplementary crystallographic data for this paper. Data can be obtained free of charge from The Cambridge Crystallographic Data Centre via [www.ccdc.cam.ac.uk/data\\_request/cif](http://www.ccdc.cam.ac.uk/data_request/cif).]

**Fluorescence lifetime measurements:** An optical parametric oscillator was pumped by a mode locked Mira titanium sapphire laser (Coherent Lasers Ltd), generating 180 fs pulses at 75 MHz and emitting light at a wavelength of 580-630nm nm. The laser was pumped by a solid state continuous wave 532 nm laser (Verdi V18, Coherent Laser Ltd), with the oscillator fundamental output of 473  $\pm$  2 nm or 405  $\pm$  2 nm. The laser beam was focused to a diffraction limited spot through a water immersion ultraviolet corrected objective (Nikon VC x60, NA1.2) and specimens illuminated at the microscope stage of a modified Nikon TE2000-U with UV transmitting optics. The focused laser spot was raster scanned using

an XY galvanometer (GSI Lumonics). Fluorescence emission was collected without de-scanning, bypassing the scanning system and passed through a colored glass (BG39) filter. The scan was operated in normal mode and line, frame and pixel clock signals were generated and synchronized with an external fast microchannel plate photomultiplier tube used as the detector (R3809-U, Hamamatsu, Japan). These were linked via a Time-Correlated Single Photon Counting (TCSPC) PCmodule SPC830 operating either under single- or two-photon(s) excitation conditions. Lifetime calculations were obtained using SPCImage analysis software (Becker and Hickl, Germany) or Edinburgh Instruments F900 TCSPC analysis software.

## Acknowledgements

SIP and SWB thank The Royal Society and STFC for funding. BYM thanks the University of Bath for a studentship (ORS). JBdS acknowledges support for a European Union Marie Curie Career Integration Grant. Rory L. Arrowsmith is thanked for the initial stages of the DFT calculations of the Zn(II)-porphyrin. Dr Amy Kieran is thanked for initial experiments in porphyrin synthesis. The authors thank EPSRC National Service for Computational Chemistry Software and High Performance Computational facilities at Imperial College London for support and computational facilities. Professors Jeremy K. M. Sanders and Paul Raithy are acknowledged for training, helpful discussions in supramolecular chemistry and porphyrin supramolecular chemistry as well as mentorship to SIP and her group. Dr. Gabriele Kociok-Köhn is thanked for assistance with X-ray diffraction. B.J.H. thanks the University of Bath for a DTC studentship. The SIP group thanks to the EPSRC for funding, as a member of the Centre of Graphene Science. The authors also acknowledge the ERC for the Consolidator Grant O2SENSE.

**Keywords:** STED Super-resolution imaging • Carbon Nanotubes • Optically Active Composite Materials • Self-Assembly • Dynamic Covalent Chemistry of Nanomaterials

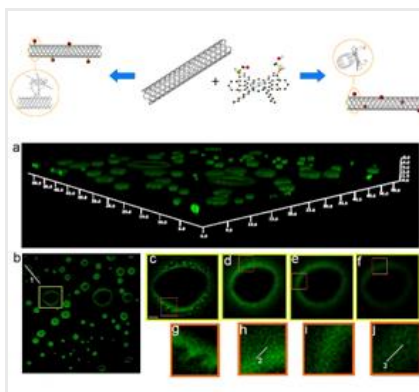
- [1] S. Iijima and T. Ichihashi, *Nature* **1993**, 363, 603-605.
- [2] a) R. H. Baughman, A. A. Zakhidov and W. A. de Heer, *Science* **2002**, 297, 787-792; b) A. Jorio, G. Dresselhaus and M. S. Dresselhaus, *Carbon nanotubes: advanced topics in the synthesis, structure, properties and applications*, Springer-Verlag Berlin Heidelberg, **2007**, p.
- [3] a) A. Hirsch, *Angew. Chem. Int. Ed.* **2002**, 41, 1853-1859; b) J. L. Bahr and J. M. Tour, *J. Mater. Chem.* **2002**, 12, 1952-1958; c) S. Niyogi, M. Hamon, H. Hu, B. Zhao, P. Bhowmik, R. Sen, M. Itkis and R. Haddon, *Acc. Chem. Res.* **2002**, 35, 1105-1113; d) C. A. Dyke and J. M. Tour, *Chem. Eur. J.* **2004**, 10, 812-817; e) M. S. Arnold, J. L. Blackburn, J. J. Crochet, S. K. Doorn, J. G. Duque, A. Mohite and H. Telg, *Phys. Chem. Chem. Phys.* **2013**, 15, 14896-14918.
- [4] a) A. Kongkanand, R. Martínez Domínguez and P. V. Kamat, *Nano Lett.* **2007**, 7, 676-680; b) S.-R. Jang, R. Vittal and K.-J. Kim, *Langmuir* **2004**, 20, 9807-9810; c) T. Hasobe, S. Fukuzumi and P. V. Kamat, *J. Phys. Chem. B.* **2006**, 110, 25477-25484; d) D. R. Barbero and S. D. Stranks, *Adv. Mater.* **2016**, 28, 9668-9685.
- [5] L. H. Tong, J.-L. Wietor, W. Clegg, P. R. Raithby, S. I. Pascu and J. K. Sanders, *Chem. Eur. J.* **2008**, 14, 3035-3044.
- [6] a) M. Alvaro, P. Atienzar, P. de la Cruz, J. L. Delgado, V. Troiani, H. Garcia, F. Langa, A. Palkar and L. Echegoyen, *J. Am. Chem. Soc.* **2006**, 128, 6626-6635; b) F. Cheng and A. Adronov, *Chem. Mater.* **2006**, 18, 5389-5391; c) S. Campidelli, C. Sooambar, E. Lozano Diz, C. Ehli, D. M. Guldi and M. Prato, *J. Am. Chem. Soc.* **2006**, 128, 12544-12552; d) T. Hasobe, S. Fukuzumi and P. V. Kamat, *J. Am. Chem. Soc.* **2005**, 127, 11884-11885.
- [7] B. Mao, D. G. Calatayud, V. Mirabello, B. J. Hodges, J. A. R. Martins, S. W. Botchway, J. M. Mitchels and S. I. Pascu, *Adv. Funct. Mater.* **2016**, 26, 634-634.

- [8] a) G. Pagona, A. S. Sandanayaka, Y. Araki, J. Fan, N. Tagmatarchis, G. Charalambidis, A. G. Coutsolelos, B. Boitrel, M. Yudasaka and S. Iijima, *Adv. Funct. Mater.* **2007**, *17*, 1705-1711; b) C. Cioffi, S. Campidelli, C. Soambar, M. Marcaccio, G. Marcolongo, M. Meneghetti, D. Paolucci, F. Paolucci, C. Ehli and G. A. Rahman, *J. Am. Chem. Soc.* **2007**, *129*, 3938-3945.
- [9] a) V. Sgobba and D. M. Guldi, *J. Mater. Chem.* **2008**, *18*, 153-157; b) V. Sgobba and D. M. Guldi, *Chem. Soc. Rev.* **2009**, *38*, 165-184.
- [10] a) L. H. Tong, P. Pengo, W. Clegg, J. P. Lowe, P. R. Raithby, J. K. M. Sanders and S. I. Pascu, *Dalton Trans.* **2011**, *40*, 10833-10842; b) L. H. Tong, J. L. Wietor, W. Clegg, P. R. Raithby, S. I. Pascu and J. K. Sanders, *Chem. Eur. J.* **2008**, *14*, 3035-3044.
- [11] a) R. Chitta, A. S. Sandanayaka, A. L. Schumacher, L. D'Souza, Y. Araki, O. Ito and F. D'Souza, *J. Phys. Chem. C* **2007**, *111*, 6947-6955; b) D. S. Hecht, R. J. Ramirez, M. Briman, E. Artukovic, K. S. Chichak, J. F. Stoddart and G. Grüner, *Nano Lett.* **2006**, *6*, 2031-2036; c) S. I. Pascu, N. Kuganathan, L. H. Tong, R. M. Jacobs, P. J. Barnard, B. T. Chu, Y. Huh, G. Tobias, C. G. Salzmann and J. K. Sanders, *J. Mater. Chem.* **2008**, *18*, 2781-2788.
- [12] J. A. Tyson, V. Mirabello, D. G. Calatayud, H. Ge, G. Kociok-Köhn, S. W. Botchway, G. Dan Pantoş and S. I. Pascu, *Adv. Funct. Mater.* **2016**, *26*, 5641-5657.
- [13] M. P. Landry, H. Ando, A. Y. Chen, J. Cao, V. I. Kottadiel, L. Chio, D. Yang, J. Dong, T. K. Lu and M. S. Strano, *Nat. Nanotechnol.* **2017**.
- [14] a) K. S. Coleman, S. R. Bailey, S. Fogden and M. L. Green, *J. Am. Chem. Soc.* **2003**, *125*, 8722-8723; b) T. Umeyama, N. Tezuka, M. Fujita, Y. Matano, N. Takeda, K. Murakoshi, K. Yoshida, S. Isoda and H. Imahori, *J. Phys. Chem. C* **2007**, *111*, 9734-9741; c) S. Banerjee, T. Hemraj - Benny and S. S. Wong, *Adv. Mater.* **2005**, *17*, 17-29.
- [15] L. J. Twyman and J. K. Sanders, *Tetrahedron Lett.* **1999**, *40*, 6681-6684.
- [16] A. W. Johnson, L. T. Kay, E. Markham, I. Price and I. B. Shaw, *J. Chem. Soc.* **1959**, 3416.
- [17] a) H. L. Anderson and J. K. Sanders, *J. Chem. Soc., Perkin Trans. 1* **1995**, 2223-2229; b) W. B. Austin, N. Bilow, W. J. Kelleghan and I. Y. Lau, *J. Org. Chem.* **1981**, *46*, 2280.
- [18] a) M. D. Pluth and K. N. Raymond, *Chem. Soc. Rev.* **2007**, *36*, 161-171; b) T. Megyes, H. Jude, T. Grósz, I. Bakó, T. Radnai, G. Tárkányi, G. Pálinskás and P. J. Stang, *J. Am. Chem. Soc.* **2005**, *127*, 10731-10738.
- [19] A. I. Oliva, K. Gomez, G. Gonzalez and P. Ballester, *New J. Chem.* **2008**, *32*, 2159-2163.
- [20] a) M. D. Peeks, T. D. W. Claridge and H. L. Anderson, *Nature* **2017**, *541*, 200-203; b) P. Neuhaus, A. Cnossen, J. Q. Gong, L. M. Herz and H. L. Anderson, *Angew. Chem. Int. Ed.* **2015**, *54*, 7344-7348; c) J. K. Sprafke, D. V. Kondratuk, M. Wykes, A. L. Thompson, M. Hoffmann, R. Drevinskas, W.-H. Chen, C. K. Yong, J. Kärnbratt, J. E. Bullock, M. Malfois, M. R. Wasielewski, B. Albinsson, L. M. Herz, D. Zigmantas, D. Beljonne and H. L. Anderson, *J. Am. Chem. Soc.* **2011**, *133*, 17262-17273; d) P. Parkinson, D. V. Kondratuk, C. Menelaou, J. Q. Gong, H. L. Anderson and L. M. Herz, *J. Phys. Chem. Lett.* **2014**, *5*, 4356-4361; e) S. Liu, D. V. Kondratuk, S. A. L. Rousseaux, G. Gil-Ramírez, M. C. O'Sullivan, J. Cremers, T. D. W. Claridge and H. L. Anderson, *Angew. Chem. Int. Ed.* **2015**, *54*, 5355-5359.
- [21] a) H. George, R. E. Palmer, Q. Guo, N. Bampos and J. K. M. Sanders, *Surf. Sci.* **2006**, *600*, 3274-3279; b) O. P. H. Vaughan, F. J. Williams, N. Bampos and R. M. Lambert, *Angew. Chem. Int. Ed.* **2006**, *45*, 3779-3781; c) Q. Guo, J. Yin, F. Yin, R. E. Palmer, N. Bampos and J. K. M. Sanders, *J. Phys. Condens. Matter* **2003**, *15*, S3127; d) V. Snitka, M. Rackaitis and R. Rodaite, *Sensor Actuat. B Chem.* **2005**, *109*, 159-166.
- [22] a) T. Palacin, H. L. Khanh, B. Joussemle, P. Jegou, A. Filoramo, C. Ehli, D. M. Guldi and S. Campidelli, *J. Am. Chem. Soc.* **2009**, *131*, 15394-15402; b) D. M. Guldi, G. M. A. Rahman, M. Prato, N. Jux, S. Qin and W. Ford, *Angew. Chem.* **2005**, *117*, 2051-2054; c) D. M. Guldi, H. Taieb, G. M. A. Rahman, N. Tagmatarchis and M. Prato, *Adv. Mater.* **2005**, *17*, 871-875; d) D. M. Guldi, G. M. A. Rahman, V. Sgobba and C. Ehli, *Chem. Soc. Rev.* **2006**, *35*, 471-487; e) C. Ehli, G. M. A. Rahman, N. Jux, D. Balbinot, D. M. Guldi, F. Paolucci, M. Marcaccio, D. Paolucci, M. Melle-Franco, F. Zerbetto, S. Campidelli and M. Prato, *J. Am. Chem. Soc.* **2006**, *128*, 11222-11231; f) D. M. Guldi, G. M. A. Rahman, N. Jux, N. Tagmatarchis and M. Prato, *Angew. Chem.* **2004**, *116*, 5642-5646; g) G. M. A. Rahman, A. Troeger, V. Sgobba, D. M. Guldi, N. Jux, D. Balbino, M. N. Tchoul, W. T. Ford, A. Mateo-Alonso and M. Prato, *Chem. Eur. J.* **2008**, *14*, 8837-8846; h) G. M. A. Rahman, D. M. Guldi, S. Campidelli and M. Prato, *J. Mater. Chem.* **2006**, *16*, 62-65; i) D. M. Guldi, G. M. A. Rahman, F. Zerbetto and M. Prato, *Acc. Chem. Res.* **2005**, *38*, 871-878.
- [23] a) P. He and M. Bayachou, *Langmuir* **2005**, *21*, 6086-6092; b) B. Zhao, H. Hu, A. Yu, D. Perea and R. C. Haddon, *J. Am. Chem. Soc.* **2005**, *127*, 8197-8203; c) Y. Qin, L. Liu, J. Shi, W. Wu, J. Zhang, Z.-X. Guo, Y. Li and D. Zhu, *Chem. Mater.* **2003**, *15*, 3256-3260; d) Y. Lin, D. E. Hill, J. Bentley, L. F. Allard and Y.-P. Sun, *J. Phys. Chem. B* **2003**, *107*, 10453-10457.
- [24] a) M. Alvaro, P. Atienzar, P. de la Cruz, J. L. Delgado, H. Garcia and F. Langa, *J. Phys. Chem. B* **2004**, *108*, 12691-12697; b) C. G. Salzmann, B. T. T. Chu, G. Tobias, S. A. Llewellyn and M. L. H. Green, *Carbon* **2007**, *45*, 907-912.
- [25] K. Jenó, Z. Viktor, K. Miklos and S. Guangyu, *New J. Phys.* **2003**, *5*, 125.
- [26] M. C. Payne, M. P. Teter, D. C. Allan, T. A. Arias and J. D. Joannopoulos, *Rev. Mod. Phys.* **1992**, *64*, 1045-1097.
- [27] Z. Hu, G. D. Pantoş, N. Kuganathan, R. L. Arrowsmith, R. M. Jacobs, G. Kociok - Köhn, J. O'Byrne, K. Jurkschat, P. Burgos, R. M. Tyrrell, S. W. Botchway, J. K. M. Sanders and S. I. Pascu, *Adv. Funct. Mater.* **2012**, *22*, 503-518.
- [28] a) L. A. De Souza, A. M. Da Silva, G. M. Junqueira, A. C. M. Carvalho and H. F. Dos Santos, *J. Mol. Struct.-THEOCHEM* **2010**, *959*, 92-100; b) V. A. Basiuk, *J. Comput. Theor. Nanosci.* **2008**, *5*, 2114-2118; c) W. Orellana and J. D. Correa, *J. Mater. Sci.* **2015**, *50*, 898-905; d) V. A. Basiuk, *J. Comput. Theor. Nanosci.* **2006**, *3*, 767-774.
- [29] E. V. Basiuk, V. A. Basiuk, P. Santiago and I. Puente-Lee, *J. Nanosci. Nanotechnol.* **2007**, *7*, 1530-1538.
- [30] N. Chen and R. T. Yang, *Carbon* **1998**, *36*, 1061-1070.
- [31] F. Rusydi, M. K. Agusta, A. G. Saputro and H. Kasai, *J. Phys. Soc. Jpn.* **2014**, *57*, 102-110.
- [32] a) M. Gallego, J. Calbo, J. Aragón, R. M. Krick Calderon, F. H. Liquido, T. Iwamoto, A. K. Greene, E. A. Jackson, E. M. Pérez, E. Ortí, D. M. Guldi, L. T. Scott and N. Martín, *Angew. Chem.* **2014**, *126*, 2202-2207; b) P. Lazar, F. Karlický, P. Jurečka, M. Kocman, E. Otyepková, K. Šafářová and M. Otyepka, *J. Am. Chem. Soc.* **2013**, *135*, 6372-6377.
- [33] a) V. Biju, T. Itoh, Y. Baba and M. Ishikawa, *J. Phys. Chem. B* **2006**, *110*, 26068-26074; b) X.-P. He, Y. Zang, T. D. James, J. Li and G.-R. Chen, *Chem. Soc. Rev.* **2015**, *44*, 4239-4248; c) E. Morales-Narváez, B. Pérez-López, L. B. Pires and A. Merkoçi, *Carbon* **2012**, *50*, 2987-2993; d) B. Pan, D. Cui, C. S. Ozkan, M. Ozkan, P. Xu, T. Huang, F. Liu, H. Chen, Q. Li, R. He and F. Gao, *J. Phys. Chem. C* **2008**, *112*, 939-944.
- [34] a) P. M. Gill, B. G. Johnson, J. A. Pople and M. J. Frisch, *Chem. Phys. Lett.* **1992**, *197*, 499-505; b) J. A. Pople, P. M. Gill and B. G. Johnson, *Chem. Phys. Lett.* **1992**, *199*, 557-560.
- [35] J. P. Perdew, K. Burke and M. Ernzerhof, *Phys. Rev. Lett.* **1996**, *77*, 3865-3868.
- [36] S. J. Grimme, *Comput. Chem.* **2006**, *27*, 1787-1799.
- [37] A. Altomare, G. Carascano, C. Giacovazzo and A. Guagliardi, *J. Appl. Crystallogr.* **1993**, *26*, 343-350.
- [38] P. W. Betteridge, J. R. Carruthers, R. I. Cooper, C. K. Prout and D. J. Watkin, *J. Appl. Crystallogr.* **2003**, *36*, 1487.
- [39] N. Walker and D. Stuart, *Acta Crystallogr., Sect. A* **1983**, *39*, 158-166.

## Entry for the Table of Contents

## FULL PAPER

**Supramolecular and covalent assemblies can influence the morphology and optical properties** of porphyrin arrays onto flat, conductive as well as insulating surfaces, and lead to the control of SWNTs functionalization at the nanoscale. The synthesis of novel functionalized luminescent single walled carbon nanotubes is reported. STED super resolution microscopy, Fluorescence Lifetime Imaging as well as XPS, TCSPC, UV-Vis, XRD, NMR, TEM and AFM probe the complexity of the emerging covalent and supramolecular aggregates.



Boyang Mao, David G. Calatayud, Vincenzo Mirabello, Haobo Ge, Benjamin J. Hodges, Robert M. J. Jacobs, Ashley M. Shepherd, José Alberto Ribeiro Martins, Navaratnarajah Kuganathan, Jorge Bernardino De La Serna, Stanley W. Botchway and Sofia I. Pascu\*

Page No. – Page No.

**Fluorescence Lifetime Imaging and Super resolution microscopies shed light on the directed- and self-assembly of functional porphyrins onto carbon nanotubes and flat surfaces**